Journal of Analytical and Applied Pyrolysis 179 (2024) 106495

Contents lists available at ScienceDirect

Journal of Analytical and Applied Pyrolysis

journal homepage: www.elsevier.com/locate/jaap

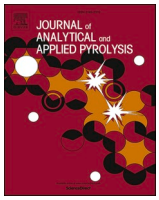

# Co-pyrolysis of waste wind turbine blades and biomass and their kinetic analysis using artificial neural network

Samy Yousef [a,*], Justas Eimontas [b], Nerijus Striūgas [b], Mohammed Ali Abdelnaby [c]

[a] Department of Production Engineering, Faculty of Mechanical Engineering and Design, Kaunas University of Technology, Kaunas LT-51424, Lithuania
[b] Lithuanian Energy Institute, Laboratory of Combustion Processes, Breslaujos 3, Kaunas LT-44403, Lithuania
[c] Mechatronics Systems Engineering Department, October University for Modern Sciences and Arts-MSA, Giza, Egypt

ARTICLE INFO

*Keywords:*
Waste wind turbine blades
Co-pyrolysis
Biomass
Artificial neural network
Kinetic analysis

ABSTRACT

This research aims to study co-pyrolysis of waste wind turbine blades (WTB) and biomass using a thermogravimetric (TG) analyser at various heating rates (10, 20, and 30 °C/min). The experiments were performed on WTB consisting of a glass fibre/unsaturated polyester resin (UPR) and woody biomass (WBs) at different mixing ratios (1:1, 2:1, 3:1 w/w). The effect of a mixing ratio and a heating rate on composition of vapours released from the co-pyrolysis process was observed using TG-FTIR and GC-MS. Also, the co-pyrolysis kinetic and thermodynamic behaviour of the WTB/WBs mixtures was studied. Meanwhile, the experimental TG curves were mathematically simulated using the Distributed activation energy method and the Independent parallel reactions, while unknown curves were predicted using an artificial neural network (ANN) model. The differential thermogravimetric results showed high compatibility between WTB and WBs (1:1 and 2:1) with a single decomposition peak, which is indicates that both feedstocks were degraded as a single-step reaction. While the higher mixing rate (3:1) revealed double decomposition peaks, indicating that the mixture undergoes two sequential decomposition reactions and several competing reactions occur simultaneously, which increases the complexity of the decomposition process. Meanwhile, the GC-MS results showed that the mixture of WTB/WBs (1:1) could significantly reduce the styrene (the main toxic compound of UPR) from 62% (in neat WTB) to 7 % at 30 °C/min. Also, presence of other aromatic hydrocarbons (benzoic acid, 2-Methoxy-4-vinylphenol, etc.) was observed in the mixture samples as a result of styrene cracking. Finally, the kinetic model-free isoconversional results showed that Ea was estimated at 275–383 kJ/mol (WBs) and 196–286 kJ/mol (WTB/WBs). Accordingly, co-pyrolysis of WTB with WBs is highly recommended to valorise WTB and eliminate their toxic styrene compound.

## 1. Introduction

Waste wind turbine blades (WTB) represent a major challenge for those working in the field of renewable energy production using wind turbines and for their sustainability due to their non-recyclability [1]. This challenge is represented by the complex and heterogeneous nature of WTB, which are mainly composed of fibres of reinforced polymer resin, which have high strength, low density and are cheaper compared to metallic materials [2]. This complex structure of WTB makes it unrecyclable and it usually ends up in landfills, which has many health and environmental concerns [3–5]. Unfortunately, this type of waste is growing very rapidly due to the large demand and is expected to reach 43 tons by 2050. In order to keep pace with the rapid growth of WTB and maximise the economic performance of it and reduce its environmental impact, recently, some effective recycling solutions have been developed to conserve materials and to integrate them into circular economy models principle [6,7]. Pyrolysis is one such promising solution that has huge potential in this regard [8,9], as it successfully recovered all WTB components by decomposing its resin fraction into oil in a nitrogen environment [10], then extracting the fibres fraction and purifying them using oxidation as a post-treatment [11]. The studies have also shown that the activation energy (Ea) required to decompose a fraction of the resin from WTB is strongly influenced by the type of resin, fibres and additives in the WTB feedstock [8,12–14].

Pyrolysis technology has been successful in treating many types of resins, such as unsaturated polyester (UPR) and epoxy, which are among the most common types of resins used in the manufacture of turbine blades [15]. However, many manufacturers prefer to rely on the UPR

* Corresponding author.
*E-mail address:* ahmed.saed@ktu.lt (S. Yousef).

https://doi.org/10.1016/j.jaap.2024.106495
Received 14 February 2024; Received in revised form 19 March 2024; Accepted 5 April 2024
Available online 8 April 2024

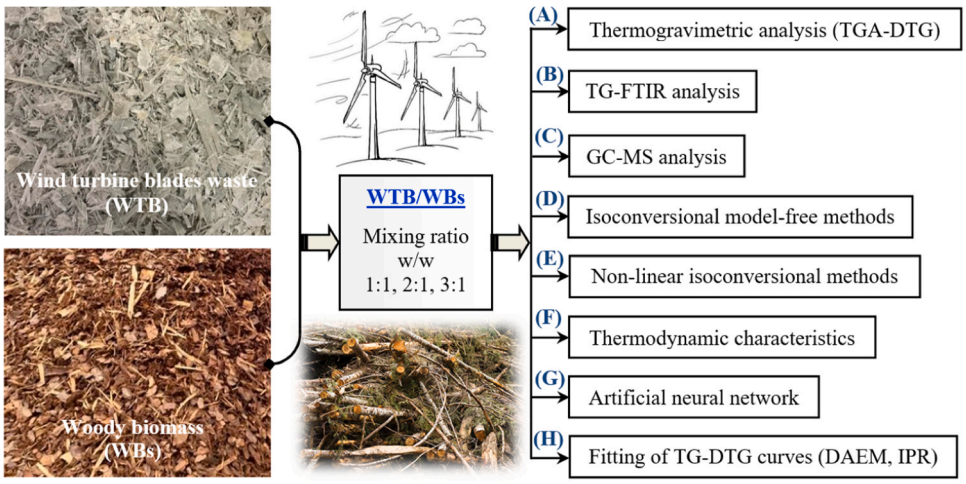


**Fig. 1.** Flowchart of the experiments and co-pyrolysis kinetics analysis of WTB/WBs.

type in further production for economic considerations [16,17]. Styrene is the main chemical compound in the UPR fraction. Recently, a pyrolysis process using thermogravimetric analysis coupled with gas chromatography-mass spectrometry (GC-MS) has been used to recover styrene from WTB (composed of carbon fibre/UPR and glass fibre/UPR) in the form of styrene-rich (62 %) vapour [18,19]. Another study also succeeded in recovering it in the form of styrene-rich oil with 48.5 % of styrene compound using a small-scale pyrolysis reactor [20]. Meanwhile, the life cycle evaluation of this recycling approach showed that this practice has a high environmental potential compared to landfills, with an improvement of up to 51 % [21]. However, styrene is a highly toxic compound that causes lung cancer [22]. Therefore, Youssef et al. [21] used two different catalysts (zeolite ZSM-5 and zeolite Y) in a pyrolysis process to crack a styrene compound into value-added aromatic chemical products consisting of 64 % benzene, toluene, and ethylbenzene compounds [23]. The Y-type catalyst also successfully reduced the amount of styrene by up to 16.2 % and reduced complexity of the reaction. Despite the promising results of catalytic pyrolysis in reducing the styrene content (as a toxic compound) in the of the produced oil, this process is very critical because as upgrading mechanism depends on the shape and size of the pores of the catalyst, which are easily blocked due to high viscosity of the produced oil and the light-density particles of char. Where the fine particles of char can settle on the surface of the catalyst and then penetrate the pores and adhere to its walls, which negatively affects the upgrading efficiency [24,25]. Therefore, this approach requires continuous recycling of catalysts to remove sediments, to open pores, or to change catalysts after a few operations [26], which requires production of more secondary solid waste that must be disposed of in landfills [27], especially since the percentage of catalysts used in the reaction is very high, reaching 50 wt% of WTB. All these limitations were a strong motivation to shift attention to the co-pyrolysis process, which can effectively contribute to improving the pyrolysis efficiency of WTB.

In this regard, co-pyrolysis of WTB over sewage sludge was investigated for the proposed carbon-enriched production without further purification [28]. The results showed high potential of the co-pyrolysis process in treating WTB. However, the process still needs to be further optimised using a rich source of aromatic substances to simplify and accelerate the reaction mechanism without producing any future residues with high selectivity for the desired chemical compounds [29]. Woody biomass (WBs) could be one of these promising sources due to its high content of cellulose, hemicelluloses, and lignin and its richness in carbohydrates and aromatic compounds. Also, WBs is characterised by its sustainability, high abundance, and carbon-neutral resources, which can help to mitigate environmental impacts and climate change. In addition, WBs was used as a powerful resource to produce clean, renewable fuels as an alternative to fossil fuels using thermochemical conversion through the pyrolysis process [30,31]. Moreover, the co-pyrolysis of WBs and different types of plastic waste (especially styrene-rich polystyrene containing chemical structures such as UPR) was studied with high conversion efficiency [32–34].

In summary, co-pyrolysis of WTB and biomass offers some potential benefits, as co-pyrolysis can lead to synergistic effects on the resulting product composition [35,36], where biomass can act as a catalyst for the pyrolysis of WTB enhancing the distribution and quality of its products [37]. In addition to its ability to reduce the oxygen content of the pyrolysis liquid product and reduce its acidity, which enhances its future utility in a sustainable energy system [38], reduces dependence on fossil fuels, and contributes to circular economy concepts as well. This approach can also help a lot in mitigating the environmental impact of WBT as biomass is classified as a renewable bio-resource [38], and thus WTB/WS co-pyrolysis helps reduce emissions and pollutants compared to typical WTB pyrolysis. In order to explore that, this research aims to study co-pyrolysis behaviour of WTB and WBs with different mixing ratios (1:1, 1:2, 1:3 w/w). The co-pyrolysis experiments were conducted using thermogravimetric (TG) analyser at three different heating rates (10, 20, 30 °C/min). The co-pyrolysis vapours generated from WTB/WBs samples were analysed using Infra-red Spectroscopy (TG-FTIR) coupled analysis and GC-MS. Also, the effect of mixing ratio on the activation energy (Ea) values was determined using free-isoconversional and nonlinear advanced kinetic techniques followed by calculating thermodynamic parameters [39,40]. Finally, artificial neural networks (ANNs) were used as an advanced machine learning approach to predict nonlinear relationships of thermogravimetric data with unknown heating rate.

## 2. Experimental and methodology

### 2.1. Feedstock preparation

The feedstocks used in the co-pyrolysis process were wood chips (WBs) and real WTB composed of fibreglass/UPR composite supplied by the European Energy company, Denmark. In order to improve the efficiency of the conversion process, both WTB and WBs feedstocks were subjected to cutting and chopping processes individually to reduce their size and prepare fine powder particles, providing particles with a high surface area that facilitate mixing of both batches and reaction during co-pyrolysis treatment. WTB and WS powder were sieved into fine particles smaller than 500 μm, and then mixed in the required proportions using an electric grinder for up to 10 min to obtain a very

homogeneous uniform distribution. The proximate and elemental analysis of both WTB and WS powder was carried out by our team previously [19]. The grounded feedstocks were intimately mixed with different mixing WTB to WBs ratios (w/w): 1:1 (WTB1), 2:1 (WTB2), and 3:1 (WTB3). In fact, the thermogravimetric analysis and pyrolysis kinetics of woods with different compositions such as chips, poplar, etc. have been extensively studied in the literature [30–32,41]. Due to the lack of similar wood feedstock with the same compositions in the current research, it was more reliable to study and analyse woody biomass available to us in order to obtain accurate results. Lastly, the overview of research plan and its methodologies are shown in Fig. 1.

### 2.2. Thermogravimetric experiments and co-pyrolysis vapour analysis

The thermal decomposition profiles of WBs and WTB/WBs samples with weight around 10 mg were investigated using TG analyser. The experiments were performed in nitrogen atmosphere as inert environment (60 mL/min) using a TA instruments, model STA449 F3; NETZSCH, Selb, Germany. This lower flow rate (60 mL/min) has been used in several studies that were dealing with similar raw materials because a higher flow rate can lead to decreased sensitivity of the analysis to small changes in terms of weight loss and detection of subtle shifts [42]. Besides, it can produce broader peaks in the measured TGA curves, incomplete evaporation or decomposition of samples, distorted kinetics, loss of volatile products, and increased consumption of nitrogen gas that must be separated from the formulated pyrolysis gas [43]. The weight loss of the mixtures was recorded with temperature change from room temperature to 900 °C at three different heating rates (10, 20, and 30 °C/min). Proteus software was then used to plot derivative thermogravimetric (DTG) curves for each mixture for all heating rates based on its TG data. These TG-DTG data were used to study the thermal decomposition, co-thermal decomposition, and thermodynamic behaviour of WTB/WBs mixtures. The TG measurements were repeated three times and successfully reproducible results were obtained. The efficiency of co-pyrolysis of WTB/WBs samples was determined using the pyrolysis index (CPI) and its formula is illustrated in Eq. (1) [44]. To assess the presence of synergy between WTB and WS blends, the theoretical and experimental weight loss of WTB/WS blends during the co-pyrolysis process were compared. The calculated weight loss ($W_{CAL}$) was estimated using Eq. (2), where $x_i$ and $w_i$ are defined as the mass fraction and weight loss of the individual mixtures (WTB and WS), respectively [37]. After that the extent of synergy was determined using Eq. (3) [45]. Finally, the composition of the vapour released from the co-pyrolysis of the specified mixture was investigated using TG-FTIR and GC-MS instruments (Shimadzu GC-2010, Kyoto, Japan).

$$\mathrm{CPI} = \frac{(-R_{\max}) \times (-R_{\mathrm{avg}}) \times M_{\mathrm{f}}}{T_{\mathrm{int}} \quad \times T_{peak} \quad \times \Delta T_{1/2}} \tag{1}$$

$$\mathrm{WCAL} = \sum x_i w_i \tag{2}$$

$$\Delta \mathrm{W} = \mathrm{W_{EXP}} - \mathrm{W_{CAL}} \tag{3}$$

### 2.3. Kinetic modelling

The pyrolysis process of mixed wastes (including WTB and WBs) is a complex mechanism involving several sequential and simultaneous reactions. Isoconversional model-free methods are among the most reliable ways to study the kinetics of this type of reactions and to determine their complexity [46]. Accordingly, Isoconversional models were employed in the present research for diagnosis of TG data of the feedstock mixtures and procurement of the kinetic parameters (pre-exponential factor "A" and conversion rate "y") using three different models (Kissinger-Akahira-Sunose "KAS", Flynn-Wall-Ozawa "FWO", and Friedman. Their formulas are expressed in Eqs. (4)–(6) [47,48]. Meanwhile, the kinetic parameters were calculated again using Vyazovkin and Cai models as nonlinear kinetic methods to improve the accuracy of the results based on optimisation process and generic algorithm, and their formulas are presented in Eqs. (7), (8), respectively [49,50]. Finally, the Distributed activation energy method (DAEM) and the independent parallel reactions (IPR) were used in the present research to fit thermogravimetric profiles of WBs and WTB/WBs samples using Eqs. (9), (10) [51,52], while their deviations (Dev.%) were checked using Eq. (11) [53].

$$\ln\left(\frac{\beta}{T^2}\right) = \ln\left(\frac{\mathrm{A}R}{Eag(y)}\right) - \frac{-Ea}{RT} \tag{4}$$

$$\ln\beta = \left(\frac{\ln \mathrm{A}Ea}{Rgy}\right) - 5.335 - \frac{1.0516Ea}{RT} \tag{5}$$

$$\ln\left(\frac{\beta dy}{dT}\right) = \ln(Af(y))\left(\frac{-Ea}{RT}\right) \tag{6}$$

$$(\alpha) = \int_0^{\alpha} \frac{dy}{f(y)} = A\int_0^{t} \exp(-E/RT)dt \tag{7}$$

$$\ln\left\{\frac{\beta_i}{T_{y,i}^2\left[h\left(x_{y,i}\right) - \frac{x_{y,i}^2 e^{x_{y,i}}}{x_{y-\Delta y,i}^2 e^{x_{y-\Delta y,i}}} h\left(x_{y-\Delta y,i}\right)\right]}\right\} = \ln\left\{\frac{A_{y-\Delta y/2}R}{E_{y-\Delta y/2} \quad g(y, y-\Delta y)}\right\} - \frac{E_{y-\Delta y/2}}{RT_{y,i}} \tag{8}$$

$$\ln\left(\frac{\beta}{T^2}\right) = \ln\left(\frac{\mathrm{A}R}{Ea}\right) + 0.6075 - \frac{Ea}{RT} \tag{9}$$

$$\frac{dm^{calc}}{dt} = -(m_0 - m)\sum_{i=1}^{3} .C_i \frac{dX_i}{dt} \tag{10}$$

$$\mathrm{Dev.}(\%) = \frac{100\sqrt{\mathrm{F.O.}_{DTG}(Z-N)}}{\max(|dm/dt|)} \tag{11}$$

### 2.4. Thermodynamic analysis

Based on the calculated kinetic parameters, the thermodynamic characteristics of the decomposed WTB/WBs mixtures were studied in terms of changing in enthalpy (ΔH), Gibbs free energy change (ΔG), and changing in entropy change (ΔS), which were calculated for the listed samples using Eqs. (12)–(14) [54]. The parameters in these equations were assigned as Boltzmann constant ($K_B$: $1.3819 \times 10^{-23}$ J/K), Planck's constant ($h$: $6.6269 \times 10^{34}$ J s), maximum decomposition temperature (Tm), and pre-exponential factor (A) received from kinetic analysis [55].

$$\Delta H = Ea - RT_m \tag{12}$$

$$\Delta \mathrm{G} = \mathrm{Ea} + RT_m \ln\left(\frac{K_B T_m}{hA}\right) \tag{13}$$

$$\Delta \mathrm{S} = \frac{\Delta H - \Delta G}{T_m} \tag{14}$$

### 2.5. Artificial neural network development

An ANN approach was developed to predict the nonlinear degradation profiles of co-pyrolysis behaviour of WTB/WBs mixtures at unknown heating rates. The architecture of the developed ANN model was built using MATLAB® software based on Levenberg-Marquardt back-propagation method because of its high accuracy in data training [56].

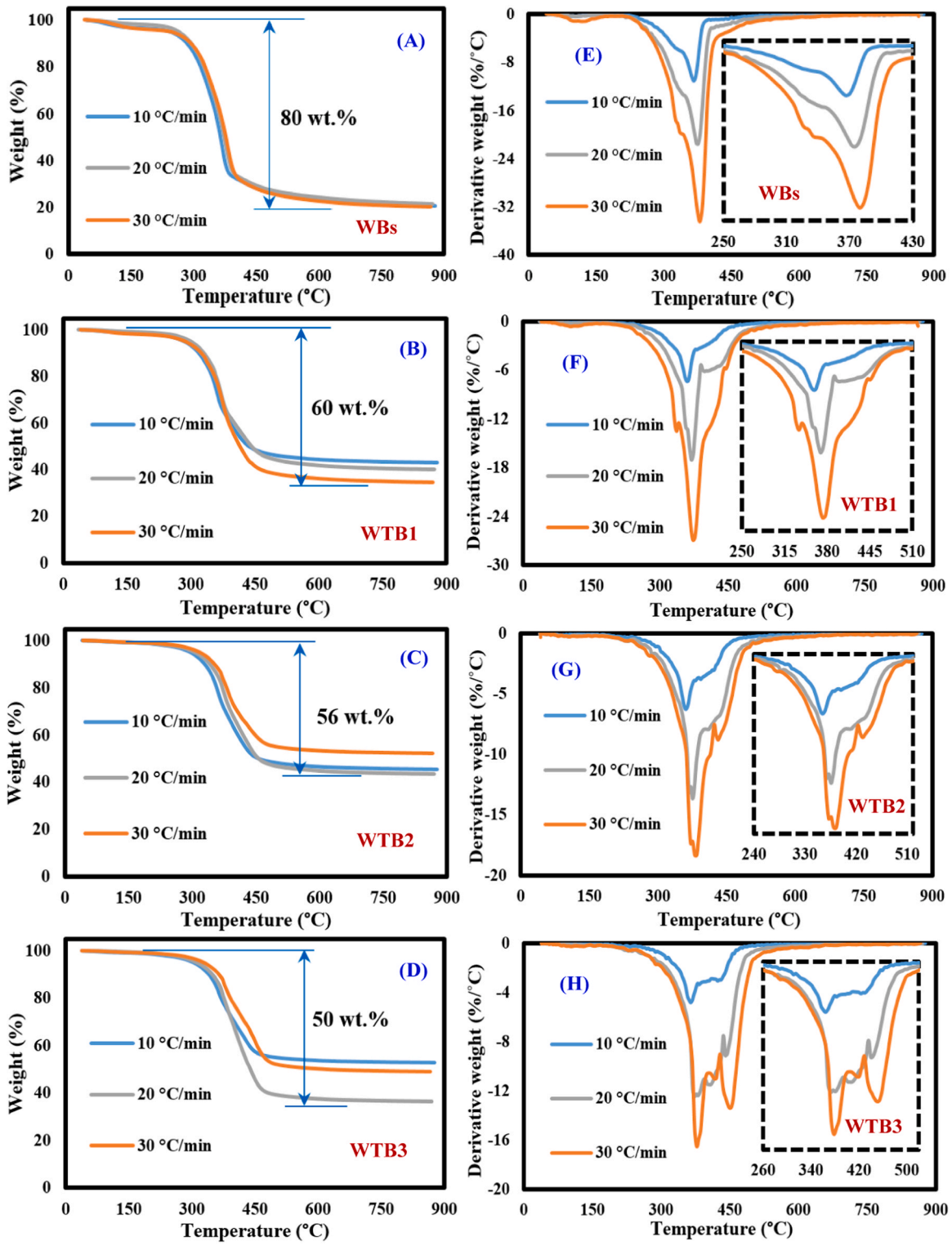


**Fig. 2.** A–D) TG and E-H) DTG curves of WBs and WTB/WBs samples.

In the developed back-propagation algorithm, input, hidden, and output layers were defined. The decomposition temperature (°C), heating condition (min/°C), and conversion rate (y) were the main input parameters, while weight loss (%) of the decomposed samples was assigned as an output of the neuron. The hidden layer was defined to create the non-linear function on the developed model [57]. This hidden layer consisted of several number of neurons selected based on maximum value of coefficient of determination ($R^2$) (between predicted and experimental TG data). The number of these hidden layers, number of their neurons, and the transfer function were determined using trial-and-error analysis based on performance criteria [58]. The performance of the developed model and its architecture were optimised under the conditions that achieved the lower values of mean square error (MSE), root mean square error (RMSE), mean absolute error (MAE), mean bias error (MBE), and higher $R^2$ values. 70 % of the build model was specified for training, while 30 % was intended for testing

**Table 1**
Co-pyrolysis characteristics of WBs and WTB/WBs samples.

| Sample | WBs | | | WTB1 | | | WTB2 | | |
|---|---|---|---|---|---|---|---|---|---|
| Heating rate (°C/min) | 10 | 20 | 30 | 10 | 20 | 30 | 10 | 20 | 30 |
| $T_{int}$ (°C) | 242 | 223 | 215 | 170 | 178 | 182 | 175 | 187 | 200 |
| $T_{peak}$ (°C) | 370 | 372 | 380 | 350 | 355 | 372 | 351 | 357 | 380 |
| $R_{max}$ (%/min) | 11.19 | 21.58 | 34.54 | 7.39 | 17.04 | 26.67 | 6.25 | 12.66 | 18.33 |
| $R_{avg}$ (%/min) | 2.78 | 1.83 | 0.92 | 2.28 | 1.40 | 0.66 | 1.67 | 1.32 | 0.63 |
| $M_f$ (%) | 20.6 | 21.2 | 20 | 43.12 | 40.04 | 34.49 | 45.53 | 43.48 | 52.09 |
| ΔT1/2 | 56 | 71 | 71 | 41 | 37 | 70 | 74 | 88 | 60 |
| CPI (%3 °$C^{-3}$ $min^{-2}$) | 1.28E-4 | 1.42E-4 | 1.10E-4 | 2.98E-4 | 4.09E-4 | 1.28E-4 | 1.05E-4 | 1.24E-4 | 1.32E-4 |
| Sample | WTB3 | | | | | | | | |
| | Peak A | | | Peak B | | | | | |
| Heating rate (°C/min) | 10 | 20 | 30 | 10 | 20 | 30 | | | |
| $T_{int}$ (°C) | 196 | 202 | 208 | 196 | 202 | 208 | | | |
| $T_{peak}$ (°C) | 352 | 274 | 378 | 423 | 446 | 450 | | | |
| $R_{max}$ (%/min) | 4.83 | 12.48 | 16.52 | 3 | 9 | 13 | | | |
| $R_{avg}$ (%/min) | 1.77 | 1.47 | 0.55 | 1.77 | 1.47 | 0.55 | | | |
| $M_f$ (%) | 52.88 | 36.6 | 49.14 | 52.88 | 36.6 | 49.14 | | | |
| ΔT1/2 | 100 | 102 | 105 | 127 | 119 | 117 | | | |
| CPI (%3 °$C^{-3}$ $min^{-2}$) | 6.55E-5 | 1.19E-4 | 5.41E-5 | 2.67E-5 | 4.52E-5 | 3.21E-5 | | | |

and validation (divided equally) [59]. Finally, the optimised model was employed to predict thermal features of WTB/WBs mixtures at 25 °C/min.

## 3. Results and discussion

### 3.1. Thermogravimetric analysis of WTB/WBs and its characteristics

Fig. 2 shows the thermal decomposition profiles of WBs and WTB/WBs samples and their decomposition features at various heating rates, while WTB had been studied before, as mentioned previously [19]. The WBs sample showed high thermal degradability with a total weight of less than 80 wt% distributed in the following manner: approximately 1 wt% loss up to 150 °C (moisture evaporation), 4 wt% up to 260 °C (hemicellulose decomposition), 61 wt% up to 400 °C (cellulose decomposition), and 14 wt% up to 600 °C (lignin decomposition) [60,61]. The WTB/WBs mixture samples showed similar features that can be described in the following way: moisture evaporation up to 150 °C followed by a small drop up to 290 °C (< 4 wt%) as a result of evaporation of the remaining chemicals in WTB and hemicellulose decomposition.

Afterwards UPR and a coat layer's sub-components of WTB started to decompose along to cellulose content of biomass up to 390 °C [19,62], followed by involvement of lignin in the reaction to achieve the full decomposition of UPR and biomass components up to 470 °C and to form ash at 600 °C [63]. Compared with the pyrolysis of WTB samples [19], WTB/WBs samples showed a lower overall weight loss of 60 wt% (WTB1), 56 wt% (WTB2), and 50 wt% (WTB3) due to high proportion of glass fibres in the feedstock, which is characterised by its high thermal resistance that allows it to remain a solid residue mixed with some char [64,65]. The decomposition profile of WTB was also affected by the heating rate and the main decomposition zone showed slightly wavering curves. Meanwhile, the DTG analysis of WBs sample showed only a single peak in the ranges of 370–380 °C (Fig. 1**C**). After mixing WTB with a small proportion of WBs (WTB1 and WTB2), this feature did not change a lot, just the maximum decomposition temperature was 345–380 °C, which means that both fractions decomposed together with high homogeneity [66]. While at the highest mixing ratio (WTB3), two peaks with different intensities were observed, meaning that WTB and WBs started to decompose separately due to reaching the saturation point. In addition, the intensity of these peaks increased with increasing heating rate because of improved heat exchange between the external surroundings of feedstock and their internal molecules [67]. All co-pyrolysis characteristics of WBs and WTB/WBs samples obtained from TG and DTG analysis are shown in Table 1. As shown, the T peak values of all samples increased with increasing heating rate. The T peak decreased when mixed with biomass. Finally, the synergistic effect of

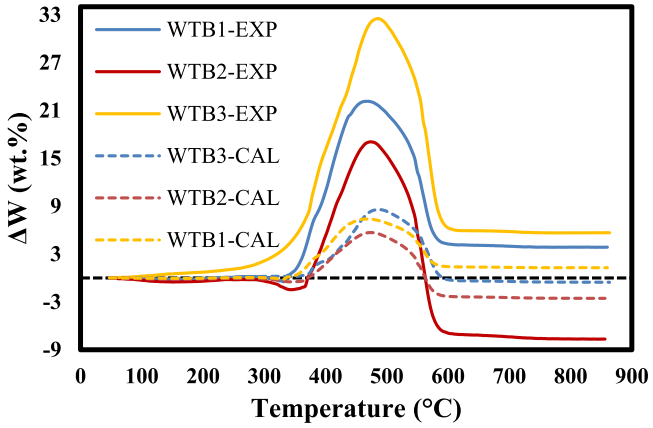


**Fig. 3.** Experimental and calculated curves of WTB/WBs samples.

WTB/WBs samples at 30 °C/min (which provides a lower amount of styrene based on GC/MS results) are shown in Fig. 3. In the fitted curves, a positive value of ΔW means that the synergistic effect is passive, while a negative value means that the synergistic effect is positive [37]. As shown, all samples showed almost positive values up to 600 °C (end of decomposition of organic components), which means that the synergistic effect is passive. Finally, the fitting error was estimated to be less than 8 %.

### 3.2. TG-FTIR analysis of the synthesised vapours

Fig. 4 shows the TG-FTIR spectra of vapours generated from co-pyrolysis of WTB/WBs mixtures at various heating rates. The 3D-FTIR spectrum of the WBs samples shows only one functional group, while the WTB1 and WTB2 samples show major spectra combined with weak spectra. This increase in weak spectra in the case of WTB3 results from decomposition of each feedstock separately and from generation of different vapours leading to conformity with the DTG results. Also, the FTIR spectra became smoother and emitted less noise when heating was increased because of decomposition of all subcomponents of WTB/WBs mixtures. The 2D TG-FTIR spectra showed five major functional groups at 830–1200 $cm^{-1}$ (aromatic hydrocarbons), 1756 $cm^{-1}$ (C═O stretching), 2348 $cm^{-1}$ (carbon dioxide clusters), 2828–2915 $cm^{-1}$ (C-H stretching vibration), and 3517 $cm^{-1}$ (hydroxyl groups). It is clear that C═O stretching and carbon dioxide clusters are the major functional groups in all samples, and the same structure was observed in the case of the WTB sample [19]. However, in case of WTB/WBs mixtures,

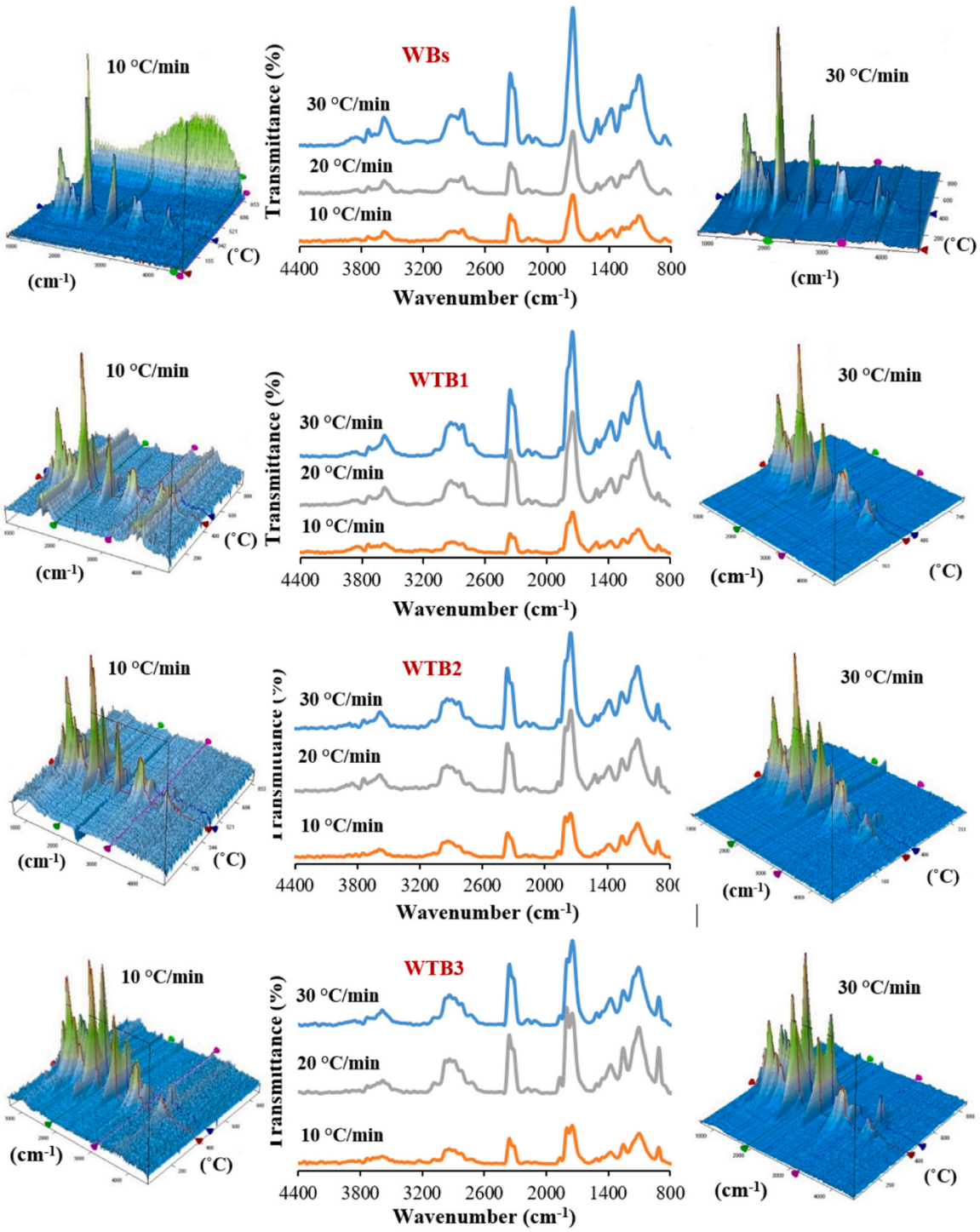


**Fig. 4.** TG-FTIR spectra of vapours resulting from co-pyrolysis of WTB/WBs samples.

co-pyrolysis vapour was very rich in aromatic hydrocarbons compounds compared with neat WTB sample, especially when the heating rate was high due to enhanced generated heat flux and its exchange between feedstock molecules [18].

### 3.3. GC-MS analysis of co-pyrolysis vapours

Fig. 5 displays GC-MS spectra of vapours resulting from co-pyrolysis of WBs and WTB/WBs samples at 10 and 30 °C/min, while the GC intensity of the vapours generated at all heating rates is summarised in Tables S1, S2 in the Supplementary materials section. The GC-MS results of WBs showed that their vapours consisted of many compounds, where acetaldehyde, hydroxy- (up to 13 %), 2-Propanone, 1-hydroxy- (9.7 %), Phenol, 2-methoxy-4-methyl- (8 %) were the predominant compounds.

The GC-MS analysis of the WTB1 sample showed a significant reduction in styrene compound in the range of 7.4 % (30 °C/min) – 13.8 % (10 °C/min) when compared with styrene compound in WTB (62 %) [19], what means that WBs succeeded to break styrene into other aromatic hydrocarbons compounds, such as benzoic acid (10.38 % at 10 °C/min) and 2-Methoxy-4-vinylphenol (9.07 % at 30 °C/min). Once the content of WBs in the feedstock started to decrease (WTB2), the intensity of styrene started to increase again in the range of 15.1 %

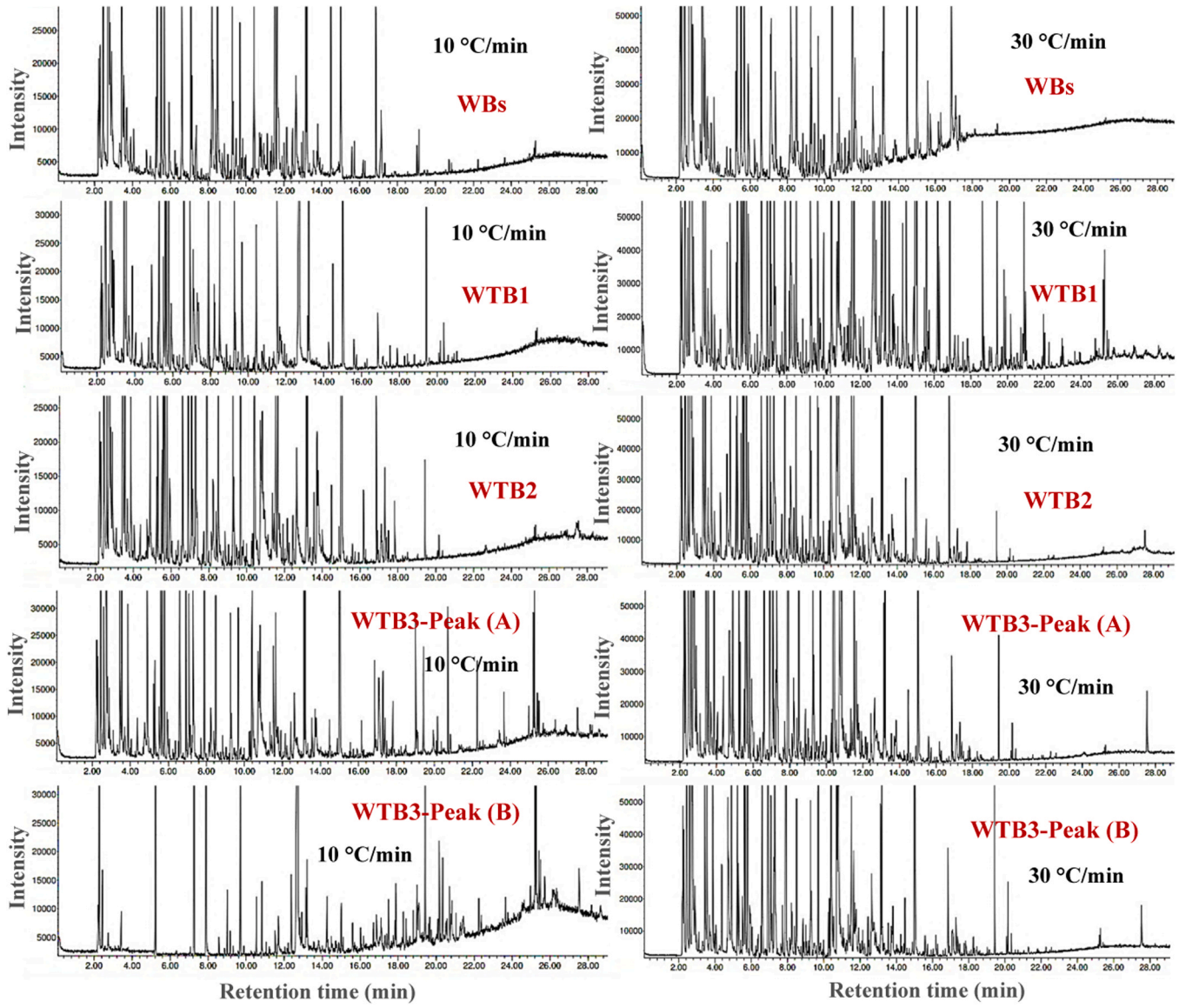


**Fig. 5.** GC/MS analysis of vapours resulting from co-pyrolysis of WTB/WBs samples.

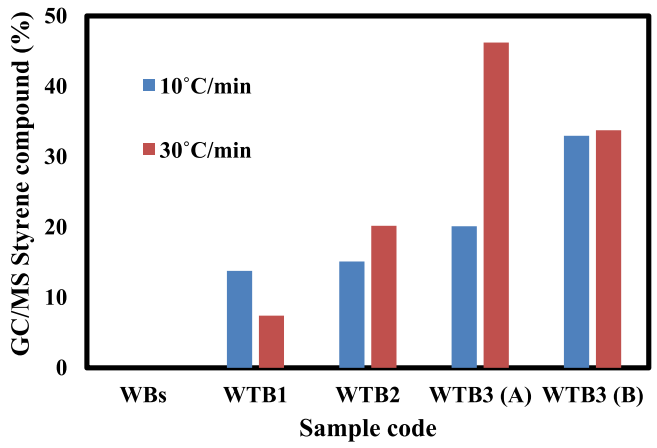


**Fig. 6.** Concentration of styrene compound in the generated vapours from WBs and WTB/WBs samples.

(10 °C/min) – 20.2 % (30 °C/min). However, the content of styrene compound was still lower than that of a neat sample which decomposed into Phthalic anhydride 29.95 % at 10°C/min-17.91 % at 30 °C/min. The same features were noticed in WTB3, where styrene's intensity was estimated in the range of 20.12 % (10 °C/min) – 46.21 % (30 °C/min) for Peak (A) and 32.98 % (10 °C/min) – 33.76 % (30°C/min) for Peak (B), as shown in Fig. 6. Also, it was observed that Phthalic anhydride content did not change a lot and was estimated at 29.31 % (10 °C/min, Peak (A)) and up to 17.57 % (30 °C/min Peak (B)). This demonstrates that WBs with low percentage can be used to decrease the amount of styrene compound in WTB and to crack it into other aromatic hydrocarbons compounds.

### 3.4. Co-pyrolysis mechanism of WTB/WBs

The studies of the pyrolysis of WTB showed that its thermal degradation mechanism is very complex because it contains several subcomponents (glass fibres, UPR, gelatine layer) [18,19]. In the present research, this complexity should be increased because more elements are included in the reaction, in particular hemicellulose, cellulose and lignin (the main component of biomass), which can all be hydrolysed

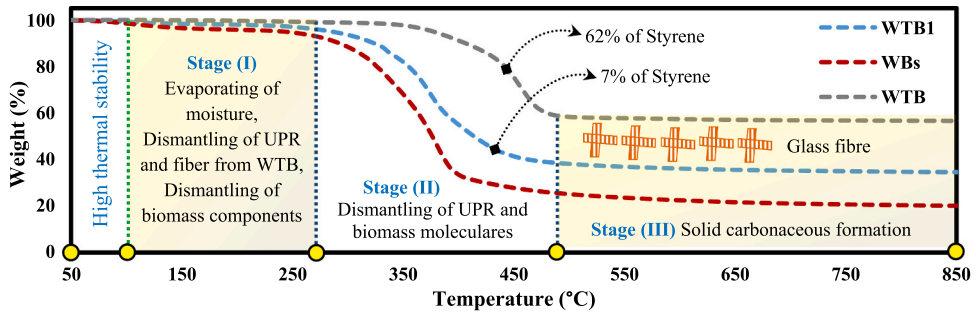


**Fig. 7.** Mechanism of WTB/WBs co-pyrolysis process.

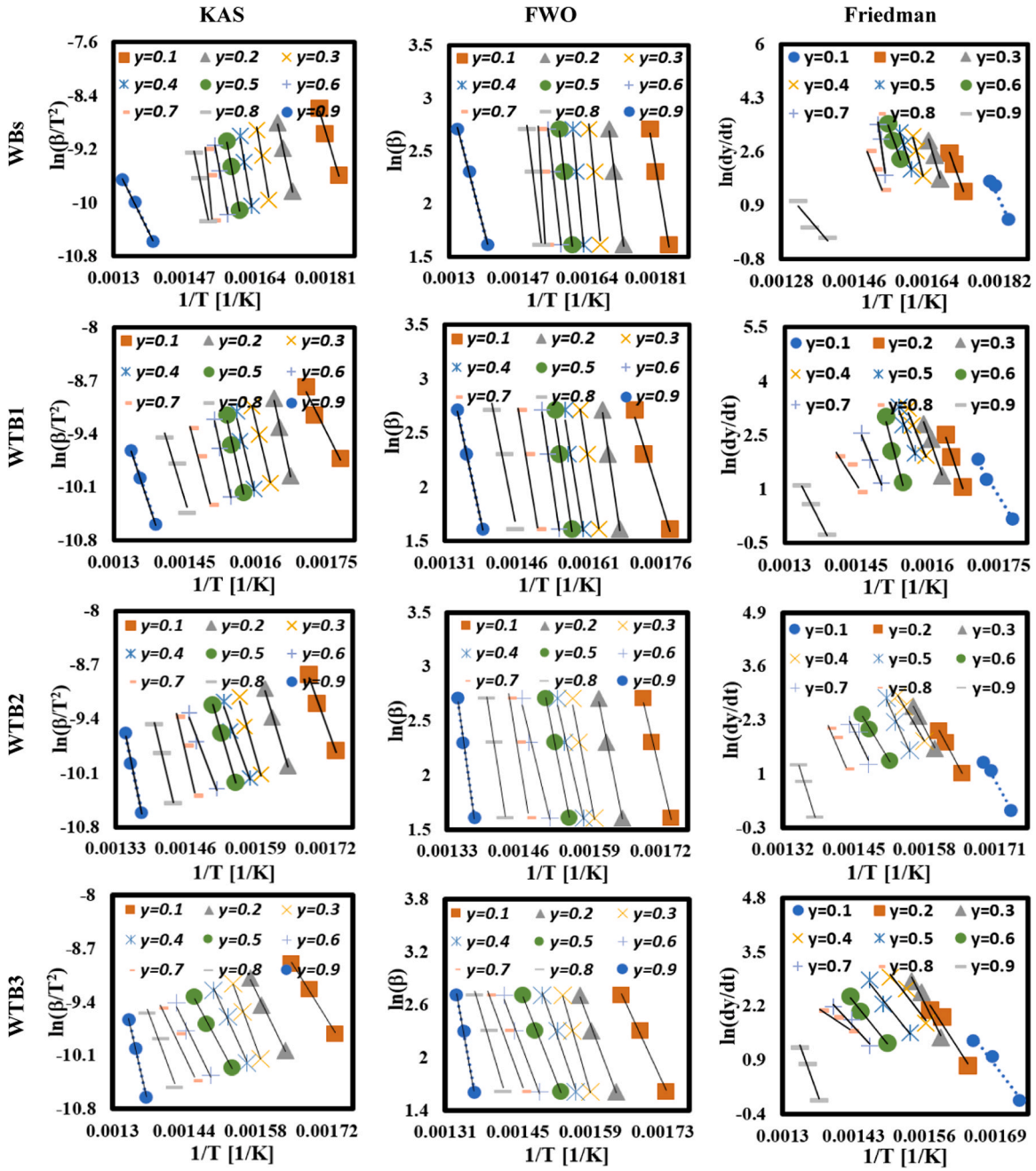


**Fig. 8.** Isoconversional model-free plots of WBs and WTB/WBs samples.

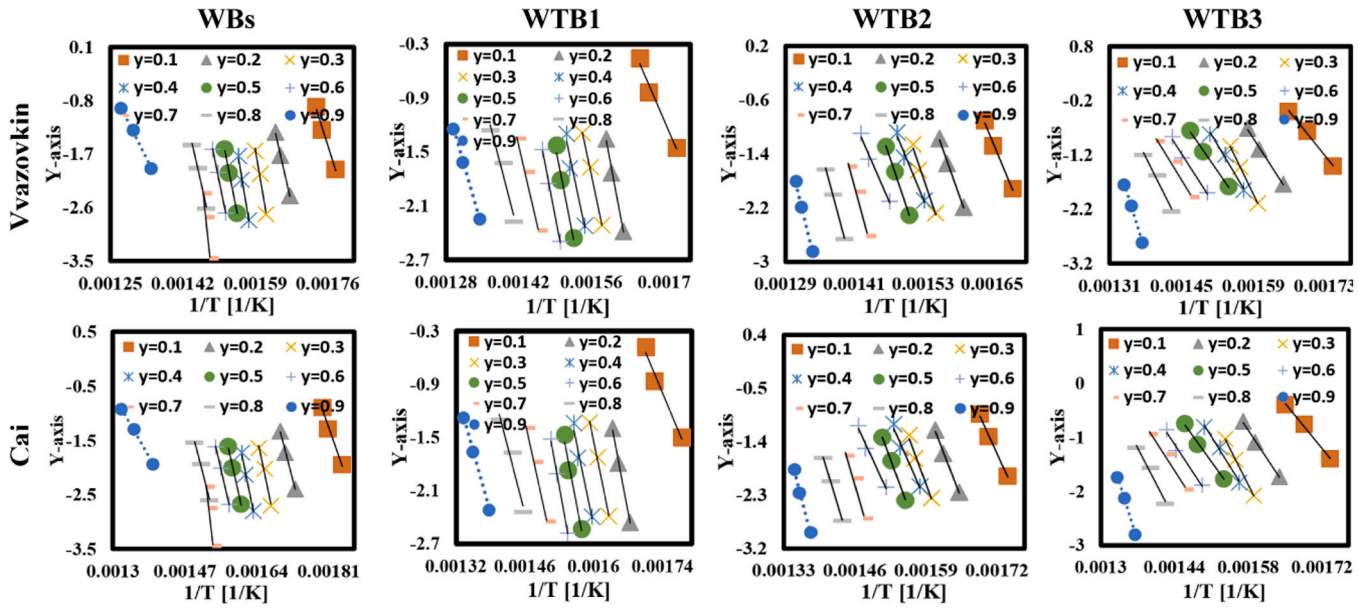


**Fig. 9.** The relationship between Ea progress and conversion rate of WBs and WTB/WBs samples.

simultaneously or sequentially. To simplify this reaction process, the thermal decomposition mechanism of WTB1 (providing lower styrene abundance) was applied based on the indicative TGA features with GC-MS results of WTB1 and compared with WBs and WTB samples [19], as shown in Fig. 7. As shown in the proposed co-pyrolysis mechanism, all samples showed high thermal stability up to 100 °C followed by three major degradation regions. In the first stage (up to 270–356 °C), the moisture began to evacuate, then the UPR and fibres of WTB were dismantled. In parallel, the components of biomass hemicellulose, cellulose and lignin were dismantled. It was observed that WBs had early degradation (270 °C) in contrast to WTB1 that reached 356 °C. In the second stage (up to 420–590 °C), the dismantled organic components of UPR and biomass were broken down into smaller molecules after overcoming their Van der Waals bonds [68], while non-degradable materials (short fibres) remained without any action due to their high thermal stability [69]. As the reaction progressed and under the effect of applied temperature, these small molecules with low crystallinity decomposed into styrene (the main compound of UPR) [70]. Meanwhile, small molecules of biomass decomposed into light hydrocarbons that can react with the styrene compound (through reforming reaction) and break it down into the original compounds [33], thus releasing more aromatic hydrocarbons, which naturally helps to get rid of the styrene compound [34,71]. Finally, after the decomposition process had finished, a short glass fibre remained in the third stage (solid carbonaceous formation) as a solid residue mixed with char fraction produced from WTB and WBs.

In summary, the mechanism of co-pyrolysis of WTB/WS involves several complex chemical reactions occurring simultaneously involving initial decomposition of WTB/WS, radical formation, cyclization, and rearrangement, which end up in the synthesis of more aromatic compounds [72]. In the first step of the reaction, the organic fraction of WTB (UPR) and WS undergo primary decomposition reactions at elevated pyrolysis temperatures that help it decompose to its main styrene compound. As the reaction progresses, the styrene compound can undergo thermal cracking to form some smaller aromatic compounds. Meanwhile, WS can be degraded to synthesise a range of volatile organic compounds (VOCs: aldehydes, ketones, acids, hydrocarbons, etc.) [73]. This is followed by radical reactions involving the cleavage of the chemical bonds of styrene and the VOCs of WS. These radicals can react together and form new chemical species. Then, some of the reactive intermediates generated by the degradation of styrene and WS can undergo cyclization and polymerisation reactions, thus eventually forming aromatic compounds. Finally, at the stage of hydrogen transfer reactions [74], numerous rearrangement reactions occur, contributing to the formation of more stable aromatic compounds from the evolving primary radicals and reactive intermediates. At a low mixing ratio (WTB1), the abundance of VOCs synthesised from WS decomposition was sufficient to contain and react with the styrene compound to produce more aromatic compounds, while at the highest mixing ratio (WTB2), the VOCs were not sufficient because they reached a point saturation as shown in Fig. 6.

### 3.5. Kinetic analysis

#### 3.5.1. Isoconversional model-free methods

First, Ea for the co-pyrolysis process of WTB/WBs samples was calculated using the listed isoconversional model-free methods above. The values of Ea at each parameter y were determined by fitting KAS, FWO, and Friedman plots (Fig. 8), then generating the slope of each model followed by calculation of Ea at each transformation stage. The KAS and FWO model-free plots showed fitted straight lines, especially at conversion rates of 20–80 %. Meanwhile, Friedman plots provided a more random distribution in the fitting lines due to their high sensitivity to experimental data of a noisy nature [75]. Fig. 9 shows the relationship between Ea progress and conversion rate, while the Ea values and their correlation coefficient factor (R2) are summarised in Table 2. Accordingly, the average Ea of WBs sample was estimated in the range of 275–383 kJ/mol. The calculations revealed that WTB/WBs samples had Ea of 196–286 kJ/mol (WTB1), 204–235 kJ/mol (WTB2), and 130–166 kJ/mol (WTB3). As shown, the average Ea value decreased gradually by increasing the amount of WTB, which means that the co-pyrolysis process can help a lot to reduce the WTB reaction's complexity, especially when compared to average Ea of WTB pyrolysis estimated at 182–228 kJ/mol [19]. However, the values calculated using model-free methods produced more variations in the results because the linear reaction did not allow to contain the feedstock on several subcomponents, hence making the reaction more of a nonlinear reaction as a result of several parallel reactions occurring at the same time [76].

In order to demonstrate the above and to increase the accuracy of the results, nonlinear kinetic modelling approaches (Vyazovkin and Cai) were used. The Ea values were computed using these approaches based

**Table 2**
The computed Ea of WBs and WTB/WBs samples at different conversion regions.

| *y* | *KAS* | *FWO* | | | *Friedman* | | | *Vyazovkin* | | | *Cai* | | |
|---|---|---|---|---|---|---|---|---|---|---|---|---|---|
| | *Ea* (kJ/mol) | $R^2$ | *A (1/s)* | *Ea* (kJ/mol) | $R^2$ | *A (1/s)* | *Ea* (kJ/mol) | $R^2$ | *A (1/s)* | *Ea* (kJ/mol) | $R^2$ | *Ea* (kJ/mol) | $R^2$ |
| **WBs sample** | | | | | | | | | | | | | |
| **0.1** | 173.76 | 0.99 | 3.93E + 14 | 201.09 | 0.99 | 1.29E + 21 | 236.06 | 0.97 | 5.18E + 23 | 177.55 | 0.99 | 183.82 | 0.99 |
| **0.2** | 239.04 | 1.00 | 2.16E + 18 | 262.29 | 1.00 | 1.92E + 25 | 306.01 | 1.00 | 2.11E + 28 | 240.18 | 1.00 | 248.67 | 0.98 |
| **0.3** | 307.86 | 0.98 | 4.26E + 23 | 340.98 | 0.10 | 1.39E + 30 | 375.95 | 0.99 | 1.53E + 33 | 306.75 | 0.98 | 317.59 | 1.00 |
| **0.4** | 315.93 | 0.99 | 6.51E + 23 | 358.46 | 0.99 | 2.13E + 30 | 402.18 | 0.99 | 4.69E + 34 | 322.30 | 0.99 | 333.69 | 0.98 |
| **0.5** | 280.93 | 1.00 | 5.14E + 19 | 314.75 | 1.00 | 1.68E + 26 | 332.23 | 1.00 | 9.18E + 27 | 280.78 | 1.00 | 290.71 | 1.00 |
| **0.6** | 270.21 | 1.00 | 1.78E + 18 | 304.26 | 1.00 | 5.81E + 24 | 306.01 | 0.98 | 1.58E + 25 | 271.24 | 1.00 | 280.82 | 1.00 |
| **0.7** | 540.41 | 1.00 | 2.49E+ 39 | 588.40 | 1.00 | 8.14E + 45 | 865.56 | 0.98 | 6.02E + 46 | 534.81 | 0.99 | 553.71 | 0.98 |
| **0.8** | 241.11 | 0.99 | 9.12E + 14 | 272.78 | 0.99 | 2.98E + 21 | 297.26 | 1.00 | 4.42E + 23 | 240.91 | 1.00 | 249.42 | 0.98 |
| **0.9** | 105.03 | 1.00 | 1.35E + 03 | 130.27 | 0.99 | 4.43E+09 | 323.49 | 0.97 | 5.99E+08 | 111.46 | 1.00 | 115.40 | 1.00 |
| **Avg.** | 274.92 | 0.99 | 2.77E + 38 | 308.14 | 0.90 | 9.05E + 44 | 382.75 | 0.99 | 6.68E + 45 | 276.22 | 0.99 | 285.98 | 0.99 |
| **WTB1 sample** | | | | | | | | | | | | | |
| **0.1** | 102.12 | 0.97 | 1.82E + 07 | 122.40 | 0.99 | 5.32E + 13 | 192.35 | 0.99 | 8.66E + 18 | 108.07 | 0.98 | 111.53 | 0.98 |
| **0.2** | 242.31 | 1.00 | 7.96E + 17 | 271.03 | 1.00 | 7.08E + 24 | 349.72 | 0.98 | 2.31E + 31 | 244.16 | 1.00 | 251.97 | 1.00 |
| **0.3** | 216.81 | 1.00 | 8.77E + 14 | 244.80 | 1.00 | 2.87E + 21 | 323.49 | 0.99 | 9.38E + 27 | 223.50 | 1.00 | 230.65 | 1.00 |
| **0.4** | 193.97 | 0.97 | 6.68E + 13 | 236.06 | 0.97 | 2.18E + 20 | 279.78 | 0.97 | 1.77E + 24 | 213.47 | 0.97 | 220.30 | 0.96 |
| **0.5** | 235.52 | 0.97 | 2.33E + 15 | 266.66 | 0.97 | 7.63E + 21 | 306.01 | 0.96 | 6.18E + 25 | 237.67 | 0.97 | 245.27 | 0.97 |
| **0.6** | 239.02 | 1.00 | 1.62E + 15 | 271.03 | 1.00 | 5.3E + 21 | 437.15 | 0.95 | 2.08E + 34 | 236.05 | 0.97 | 243.60 | 0.99 |
| **0.7** | 200.94 | 1.00 | 2.95E + 12 | 227.32 | 1.00 | 1.31E + 18 | 279.78 | 0.98 | 1.06E + 22 | 204.24 | 0.96 | 210.78 | 1.00 |
| **0.8** | 172.62 | 0.95 | 2.79E + 08 | 201.09 | 0.95 | 2.48E + 15 | 174.86 | 0.97 | 4.54E + 13 | 176.11 | 0.95 | 181.74 | 0.96 |
| **0.9** | 156.22 | 1.00 | 4.04E + 06 | 183.60 | 1.00 | 1.32E + 13 | 227.00 | 1.00 | 1.45E + 16 | 161.10 | 1.00 | 166.26 | 1.00 |
| **Avg.** | 195.50 | 0.98 | 8.90E + 16 | 224.89 | 0.99 | 7.88E + 23 | 285.57 | 0.98 | 2.32E + 33 | 200.49 | 0.98 | 206.90 | 0.98 |
| **WTB2 sample** | | | | | | | | | | | | | |
| **0.1** | 160.71 | 0.99 | 9.74E + 11 | 183.60 | 0.99 | 8.66E + 18 | 201.09 | 0.98 | 6.4E + 19 | 164.44 | 0.98 | 170.25 | 0.98 |
| **0.2** | 193.52 | 0.99 | 3.62E + 13 | 218.58 | 1.00 | 1.18E + 20 | 209.83 | 1.00 | 4.35E + 19 | 196.29 | 1.00 | 203.22 | 1.00 |
| **0.3** | 201.20 | 0.98 | 1.61E + 13 | 227.32 | 0.98 | 5.25E + 19 | 218.58 | 1.00 | 1.93E + 19 | 203.85 | 0.97 | 211.04 | 1.00 |
| **0.4** | 162.95 | 0.98 | 1.22E + 12 | 183.60 | 0.98 | 2.69E + 16 | 192.35 | 1.00 | 7.32E + 16 | 166.59 | 1.00 | 172.47 | 0.97 |
| **0.5** | 197.87 | 1.00 | 9.66E + 07 | 227.32 | 1.00 | 6.96E + 18 | 253.55 | 0.99 | 1.03E + 21 | 200.76 | 0.97 | 207.85 | 0.97 |
| **0.6** | 153.81 | 0.98 | 5.96E + 14 | 174.86 | 0.98 | 5.96E + 14 | 183.60 | 0.99 | 5.96E + 14 | 157.64 | 0.98 | 163.20 | 0.97 |
| **0.7** | 248.59 | 0.98 | 1.61E + 14 | 279.78 | 0.98 | 3.89E + 21 | 236.06 | 0.99 | 3.55E + 18 | 250.25 | 0.97 | 259.09 | 0.96 |
| **0.8** | 248.59 | 1.00 | 1.23E + 14 | 279.78 | 0.99 | 4.03E + 20 | 253.55 | 0.96 | 7.39E + 18 | 249.83 | 0.99 | 258.65 | 0.95 |
| **0.9** | 266.05 | 1.00 | 8.66E + 20 | 314.75 | 1.00 | 1.74E + 22 | 367.21 | 0.96 | 5.19E + 25 | 282.67 | 1.00 | 292.65 | 1.00 |
| **Avg.** | 203.70 | 0.99 | 9.63E + 19 | 232.18 | 0.99 | 2.43E + 21 | 235.09 | 0.99 | 5.76E + 24 | 208.04 | 0.98 | 215.38 | 0.98 |
| **WTB3 sample** | | | | | | | | | | | | | |
| **0.1** | 88.59 | 0.99 | 2.98E + 05 | 113.66 | 1.00 | 2.65E + 12 | 148.63 | 0.97 | 3.93133E + 14 | 96.58 | 1.00 | 97.99 | 1.00 |
| **0.2** | 111.67 | 1.00 | 4.07E + 06 | 139.89 | 1.00 | 1.33E + 13 | 174.86 | 0.95 | 1.45865E + 16 | 119.44 | 1.00 | 121.18 | 1.00 |
| **0.3** | 149.65 | 1.00 | 7.30E + 08 | 174.86 | 1.00 | 6.48E + 15 | 218.58 | 0.97 | 1.93253E + 19 | 158.36 | 1.00 | 160.67 | 1.00 |

(*continued on next page*)

**Table 2** (*continued*)

| *y* | *KAS* | *FWO* | | | *Friedman* | | | *Vyazovkin* | | | *Cai* | | |
|---|---|---|---|---|---|---|---|---|---|---|---|---|---|
| | *Ea* (kJ/mol) | $R^2$ | *A (1/s)* | *Ea* (kJ/mol) | $R^2$ | *A (1/s)* | *Ea* (kJ/mol) | $R^2$ | *A (1/s)* | *Ea* (kJ/mol) | $R^2$ | *Ea* (kJ/mol) | $R^2$ |
| **0.4** | 116.40 | 0.99 | 2.77E + 06 | 148.63 | 0.99 | 3.33E + 12 | 139.89 | 0.95 | 9.03911E + 12 | 129.26 | 1.00 | 131.15 | 0.98 |
| **0.5** | 99.77 | 0.98 | 3.24E + 04 | 131.15 | 1.00 | 1.06E + 11 | 148.63 | 0.98 | 2.12819E + 12 | 111.66 | 1.00 | 113.29 | 1.00 |
| **0.6** | 108.08 | 0.97 | 6.12E + 04 | 131.15 | 0.99 | 2.00E + 11 | 139.89 | 1.00 | 2.00014E + 11 | 119.61 | 1.00 | 121.35 | 1.00 |
| **0.7** | 116.40 | 0.97 | 4.50E + 04 | 139.89 | 0.98 | 1.47E + 11 | 122.40 | 0.96 | 7,316,148,666 | 124.96 | 0.97 | 126.78 | 0.97 |
| **0.8** | 141.34 | 1.00 | 1.88E + 06 | 174.86 | 0.98 | 1.67E + 13 | 78.69 | 0.96 | 1,879,069.194 | 156.13 | 0.97 | 158.41 | 0.98 |
| **0.9** | 241.11 | 1.00 | 4.85E + 12 | 279.78 | 1.00 | 4.31E + 19 | 323.49 | 1.00 | 1.73994E + 22 | 252.64 | 0.99 | 256.32 | 1.00 |
| **Avg.** | 130.33 | 0.99 | 5.39E + 11 | 159.32 | 0.99 | 4.79E + 18 | 166.12 | 0.97 | 1.93541E + 21 | 140.96 | 0.99 | 143.01 | 0.99 |

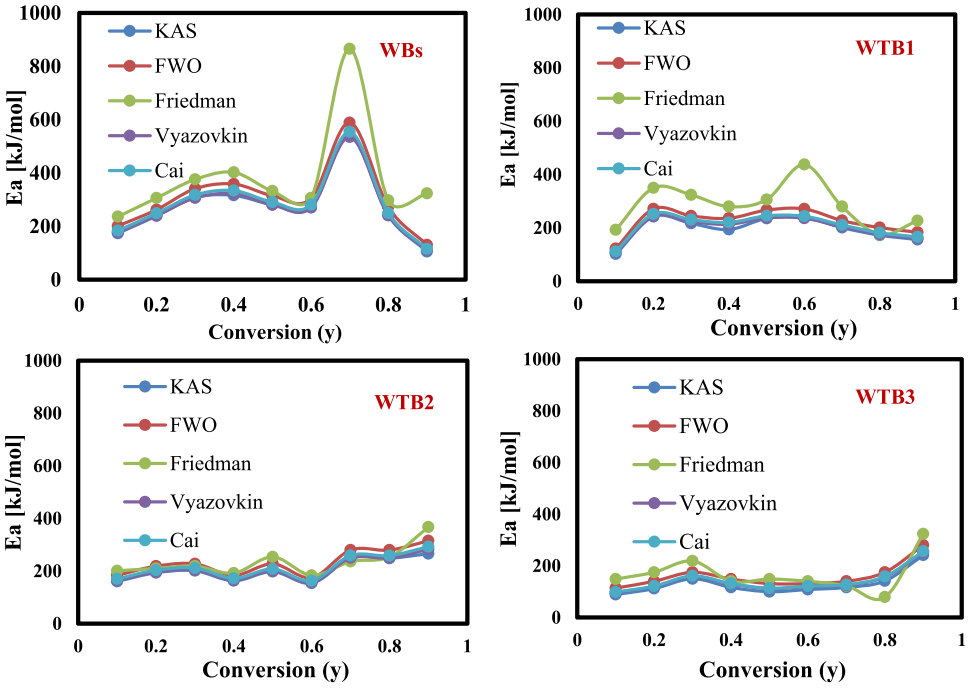


**Fig. 10.** Vyazovkin and Cai plots of curves of WBs and WTB/WBs samples.

**Table 3**
Thermodynamic coefficients of parameters of WTB/WBs sample at 30℃/min.

| *y* | *KAS* | | | *FWO* | | | *Friedman* | | |
|---|---|---|---|---|---|---|---|---|---|
| | ΔH (kJ/mol) | ΔG (kJ/mol) | ΔS (J/mol K) | ΔH (kJ/mol) | ΔG (kJ/mol) | ΔS (J/mol K) | ΔH (kJ/mol) | ΔG (kJ/mol) | ΔS (J/mol K) |
| 0.1 | 97 | 175 | 150 | 117 | 115 | 181 | 187 | 121 | 290 |
| 0.2 | 237 | 183 | 367 | 266 | 126 | 412 | 344 | 125 | 534 |
| 0.3 | 211 | 194 | 328 | 239 | 142 | 371 | 318 | 140 | 493 |
| 0.4 | 189 | 185 | 292 | 231 | 147 | 357 | 274 | 142 | 425 |
| 0.5 | 230 | 208 | 357 | 261 | 159 | 405 | 301 | 150 | 466 |
| 0.6 | 234 | 213 | 362 | 266 | 165 | 412 | 432 | 176 | 669 |
| 0.7 | 196 | 209 | 303 | 222 | 166 | 344 | 274 | 170 | 425 |
| 0.8 | 167 | 230 | 259 | 196 | 173 | 303 | 169 | 168 | 263 |
| 0.9 | 151 | 237 | 234 | 178 | 184 | 276 | 222 | 190 | 343 |
| Avg. | 190 | 204 | 294 | 220 | 153 | 340 | 280 | 153 | 434 |

on integration optimisation algorithms built with Matlab software. After several iterations, the Ea values became constant, thus the optimal Ea was estimated mathematically for each model, where the average Ea was estimated at 276.22–285.98 kJ/mol (WBs), 200.49–206.90 kJ/mol (WTB1), 208.04–215.38 kJ/mol (WTB2), and 140.96–143.01 kJ/mol (WTB3) with $R^2 \geq 0.98$ (Table 2). Finally, the Vyazovkin and Cai relationships were plotted and the plots of WBs and WTB/WBs samples are shown in Fig. 10, while their Y-axes formulas are described using Eqs.

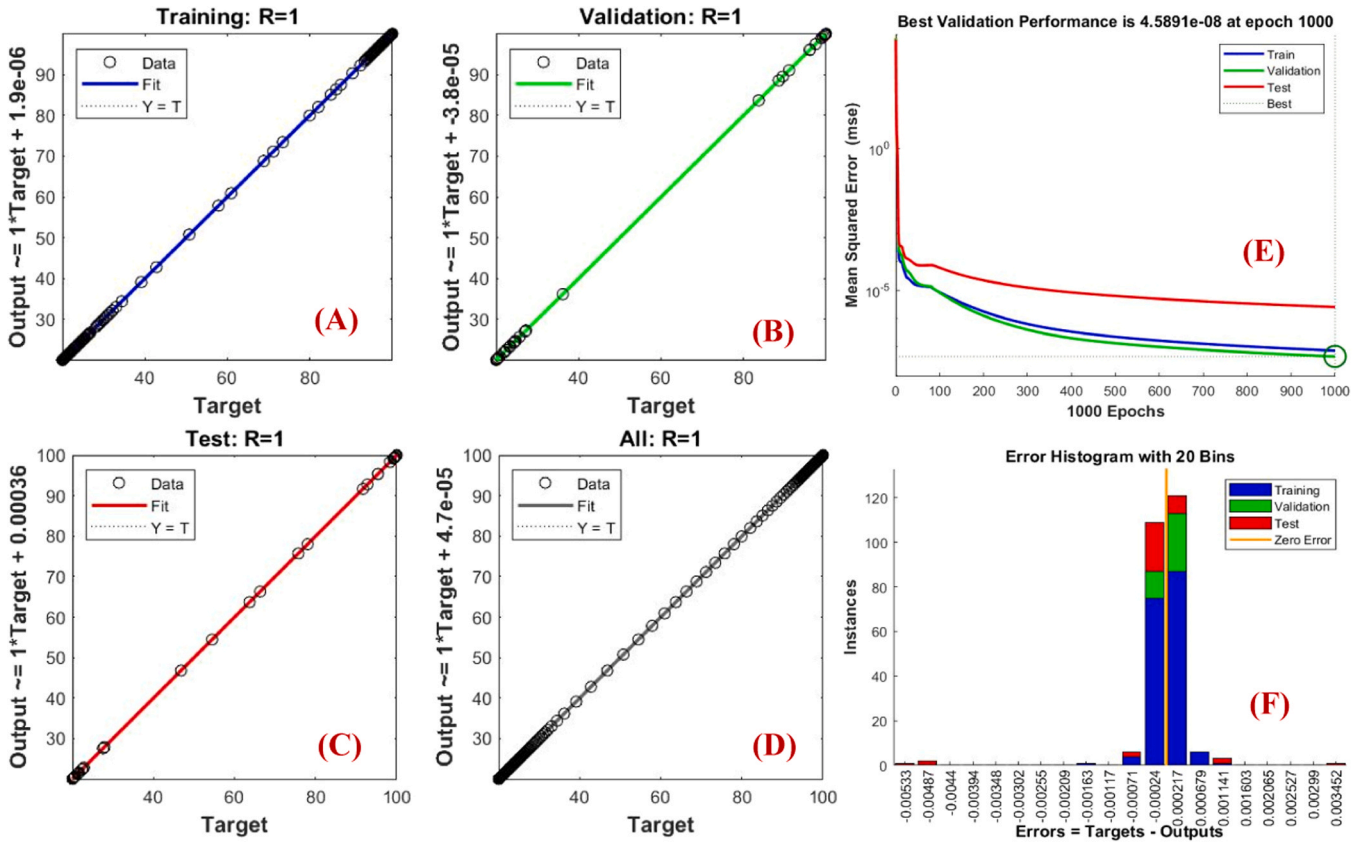


**Fig. 11.** The ANN-predicted relationships of WBs pyrolysis at 30 °C/min.

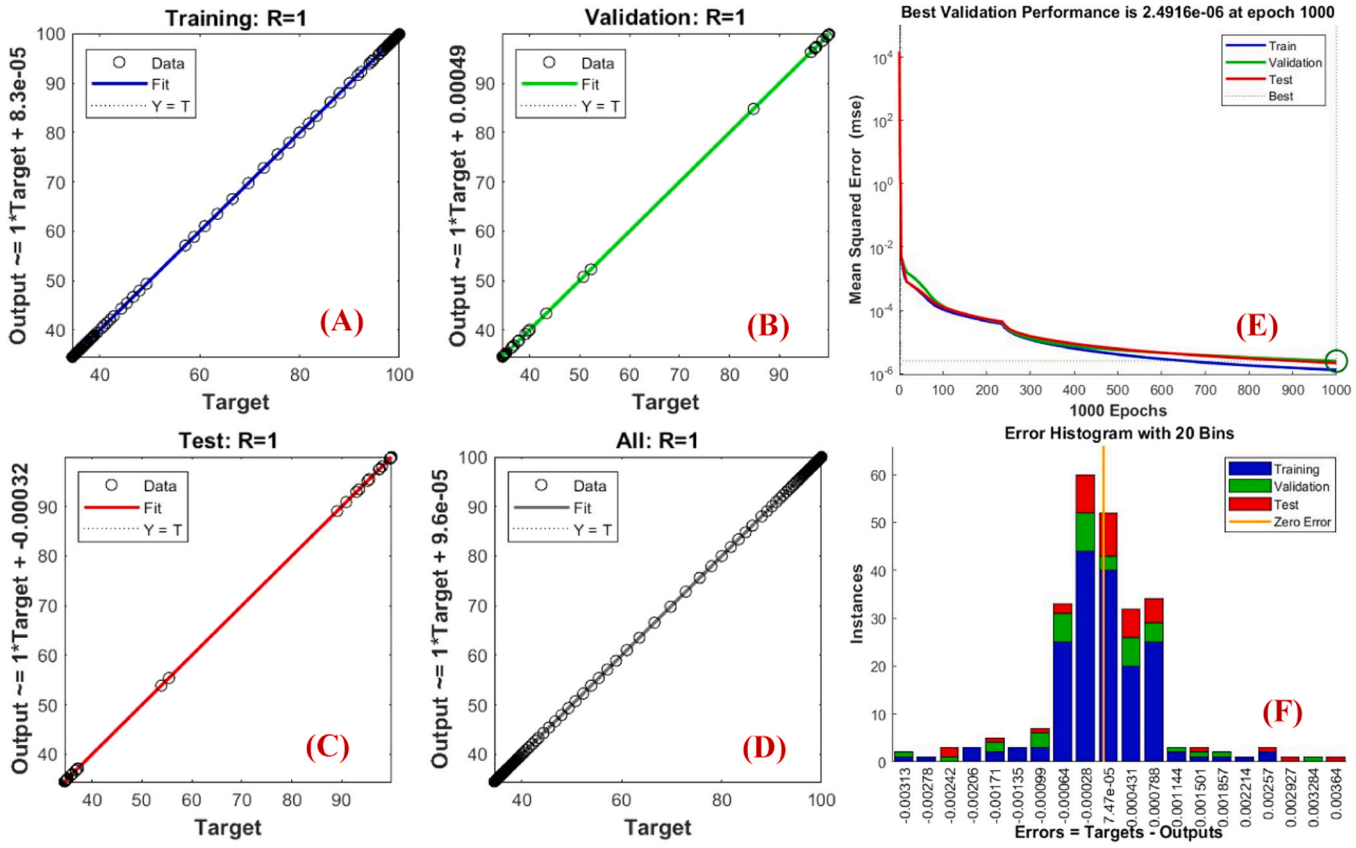


**Fig. 12.** The ANN predicted relationships of WTB/WBs co-pyrolysis at 30 °C/min.

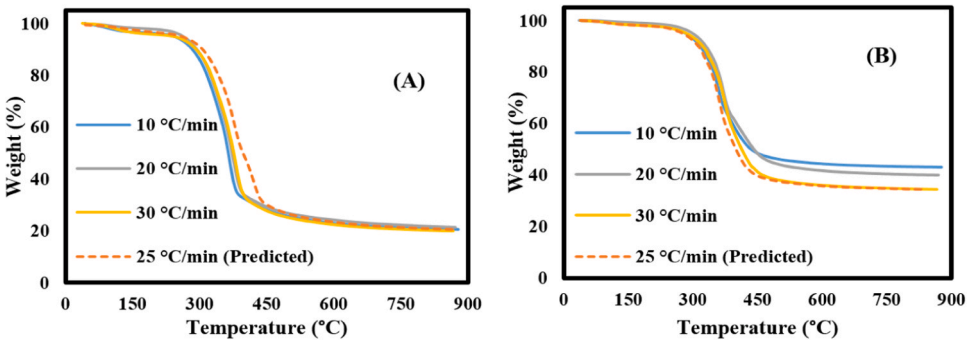


**Fig. 13.** The TGA experimental and ANN-predicted data for A) WBs and B) WTB1 samples.

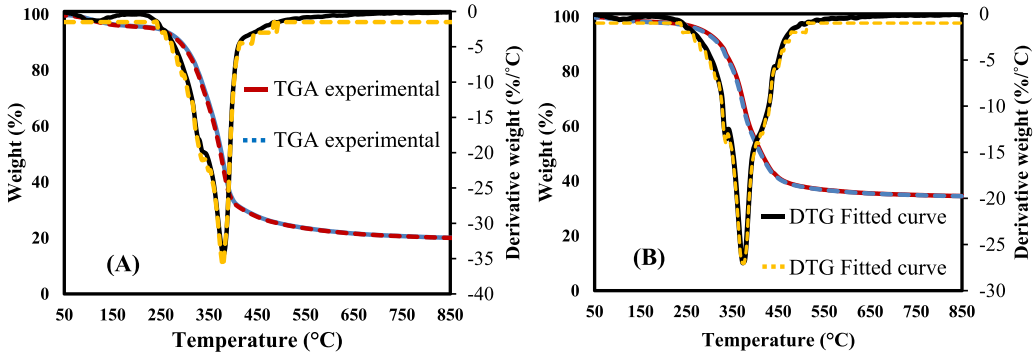


**Fig. 14.** Fitting of TGA and DTG profiles of A) WBs and B) WTB1 at 30 °C/min.

(S1) and (S2) in the Supplementary section. Lastly, the calculated thermodynamic parameters of WTB/WBs sample at 30 °C/min providing less styrene compound are summarised in Table 3.

### 3.6. ANN-based prediction of co-pyrolytic behaviour

The constructed ANN model was employed to predict TGA-measured data of WBs and WTB1 samples (optimal mixing ratio) at unknown heating conditions. The optimisation process showed that two hidden layers with neurons with a 3 × 5 × 1 pattern were more stable and had the best prediction performance. Figs. 11, 12 shows the ANN-predicted diagrams of WBS and WTB1 co-pyrolysis at 30 °C/min, respectively. It is clear that the training (Fig. 11**A**, 12**A)** and validation Figs. 11**B**, 12**B** models were successful in prediction and validation of co-pyrolytic behaviour of both samples (WBs and WTB1) with R2 = 1. Meanwhile. the accuracy error distribution of the developed network and their regressions showed a high accuracy, as shown in Fig. 11**C**, 12**D** and Fig. 11**C**, 12**D**.

In the meantime, the MSE was estimated to be 4.5891 E-08 in case of WBs **(**Fig. 11**E)** and 2.4916 E-06 in case of WTB1 **(**Fig. 12**E)** after 1000 iterations. Meanwhile, the basic characteristics of error distribution **((**Fig. 11**F)** and **(**Fig. 12**F)** tended to follow a normal distribution behaviour around zero and were in the ranges of − 0.000024 + 0.0000217 (WBs) and − 0.00028 + 7.47E-05 (WTB1). Finally, the ANN model built at the optimal conditions was used to predict the TGA curves of both samples at 25 °C/min, followed by comparison with the experimental data, as shown in Fig. 13. It appears that an optimised ANN model with good performance was used to learn and predict the mass loss behaviour of WBs and the pyrolytic decomposition behaviour of WTB1 samples at unspecified heating rates. However, the predicted TGA profiles were imaged at 25 °C/min for WBs and WTB1, exceeding those at 30 and 20 °C/min. This is due to the complexity of the structural composition of these raw materials (WBs and WTB1), which needs further optimisation process of the developed ANN to improve the accuracy of the results. Based on that a well-trained ANN can be employed to predict more TGA data of WTB/WBs mixture and other types of mixtures.

**Table 4**
DAEM and IPR optimum parameters of WBs and WTB1 pyrolysis samples.

| Parameter | WBs | | WTB1 | |
|---|---|---|---|---|
| | DAEM | IPR | DAEM | IPR |
| E1 | 307.77 | 200.17 | 225.32 | 146.54 |
| A1 | 4.43E + 43 | 7.39E + 38 | 3.2E + 22 | 5.34E + 17 |
| E2 | 144.66 | 136.63 | 144.67 | 136.63 |
| A2 | 4.43E+56 | 1.7E+53 | 3.2E + 35 | 1.22E + 32 |

### 3.7. Fitting of TGA-DTG curves of WBs and WTB/WBs samples

The distinctive characteristics of TGA and DTG experimental profiles of WBs (at 30 °C/min) and WTB1 (at 30 °C/min) samples were fitted using DAEM and IPR, respectively. The simulated profiles and their validated experimental TGA-DTG curves are shown Fig. 14**.** As shown, both DARK and IPR models succeeded to fit the distinctive region of WBs and WTB/WBs samples with deviation close to zero. The activation energies and pre-exponential factors using the fitting process are summarised in Table 4.

## 4. Conclusions

In this research, the co-pyrolysis behaviour of WTB (glass fibre/UPR)/woody biomass (WBs)) and their volatile products was studied and analysed. The kinetic and thermodynamic behaviour of co-pyrolysis of WTB/WBs with different mixing ratio was also studied. The measured TG curves at unspecified heating rates were fitted mathematically using an ANN model. The TG-DTG results showed that the WTB/WBs mixture decomposed together at a single peak up to the mixing ratio (WTB:

WBs) = 1:1, while at a higher mixing ratio, each fraction (WTB and WBs) in the feedstock started to decompose separately. Also, the WTB/WBs sample with a 1:1 mixing ratio was successful in cracking the styrene compound (the main toxic element in WTB) upto 7 % at 30 °C/min, in addition to developing other more aromatic hydrocarbon compounds. At this mixing ratio, the activation energy was estimated at 195.5 kJ/mol (KAS), 224.9 kJ/mol (FWO), 285.6 kJ/mol (Friedman), 200.5 kJ/mol (Vyazovkin), 206.9 kJ/mol (Cai) with R2 $\geq$ 0.98. Based on these results, it can be confirmed that the co-pyrolysis process has high potential in WTB treatment and reduction of its toxic substrates in pyrolysis products. Finally, based on the results obtained, the co-pyrolysis of WTB and WTS mixture can be considered as a promising approach for production of sustainable energy.

## CRediT authorship contribution statement

**Justas Eimontas:** Formal analysis, Data curation, Conceptualization. **Samy Yousef:** Writing – review & editing, Writing – original draft, Visualization, Validation, Supervision, Software, Resources, Project administration, Methodology, Investigation, Funding acquisition, Formal analysis, Data curation, Conceptualization. **Nerijus Striūgas:** Software, Resources, Formal analysis, Data curation, Conceptualization. **Moh Abdelnaby:** Formal analysis, Data curation, Conceptualization, Methodology, Software.

## Declaration of Competing Interest

The authors declare that they have no known competing financial interests or personal relationships that could have appeared to influence the work reported in this paper.

## Data availability

The data that has been used is confidential.

## Acknowledgment

This project has received funding from the Research Council of Lithuania (LMTLT), Agreement no. S-MIP-23-118.

## Appendix A. Supporting information

Supplementary data associated with this article can be found in the online version at doi:10.1016/j.jaap.2024.106495.

## References

[1] N. Rathore, N.L. Panwar, Environmental impact and waste recycling technologies for modern wind turbines: an overview, Waste Manag. Res. 41 (4) (2022) 744–759, https://doi.org/10.1177/0734242x221135527.
[2] R. Fonte, G. Xydis, Wind turbine blade recycling: an evaluation of the European market potential for recycled composite materials, J. Environ. Manag. 287 (2021) 112269, https://doi.org/10.1016/j.jenvman.2021.112269.
[3] J. Beauson, A. Laurent, D.P. Rudolph, J.P. Jensen, The complex end-of-life of wind turbine blades: a review of the European context, Renew. Sustain. Energy Rev. 155 (2022) 111847, https://doi.org/10.1016/j.rser.2021.111847.
[4] M.Y. Khalid, Z.U. Arif, M. Hossain, R. Umer, Recycling of wind turbine blades through modern recycling technologies: a road to zero waste, Renew. Energy Focus 44 (2023) 373–389, https://doi.org/10.1016/j.ref.2023.02.001.
[5] A. Nagle, E.L. Delaney, L.C. Bank, P. Leahy, A comparative life cycle assessment between landfilling and co-processing of waste from decommissioned Irish wind turbine blades, J. Clean. Prod. 277 (2020) 123321, https://doi.org/10.1016/j.jclepro.2020.123321.
[6] M.J. Leon, Recycling of wind turbine blades: recent developments, Curr. Opin. Green Sustain. Chem. 39 (2023) 100746, https://doi.org/10.1016/j.cogsc.2022.100746.
[7] G. Lichtenegger, A. Rentizelas, N.L. Trivyza, S. Siegl, Offshore and onshore wind turbine blade waste material forecast at a regional level in Europe until 2050, Waste Manag. 106 (2020) 120–131, https://doi.org/10.1016/j.wasman.2020.03.018.
[8] W. Chen, M. Ye, M. Li, B. Xi, J. Hou, X. Qi, J. Zhang, Y. Wei, F. Meng, Characteristics, kinetics and product distribution on pyrolysis process for waste wind turbine blades, J. Anal. Appl. Pyrolysis 169 (2023) 105859, https://doi.org/10.1016/j.jaap.2023.105859.
[9] S. Yousef, V. Lekavičius, N. Striūgas, Techno-economic analysis of thermochemical conversion of waste masks generated in the EU during COVID-19 pandemic into energy products, Energies 16 (9) (2023) 3948, https://doi.org/10.3390/en16093948.
[10] M. Shen, Z. Guo, W. Feng, A study on the characteristics and thermal properties of modified regenerated carbon fiber reinforced thermoplastic composite recycled from waste wind turbine blade spar, Compos. Part B: Eng. 264 (2023) 110878, https://doi.org/10.1016/j.compositesb.2023.110878.
[11] M. Xu, H. Ji, Y. Wu, J. Di, X. Meng, H. Jiang, Q. Lü, The pyrolysis of end-of-life wind turbine blades under different atmospheres and their effects on the recovered glass fibers, Compos. Part B: Eng. 251 (2023) 110493, https://doi.org/10.1016/j.compositesb.2022.110493.
[12] L. Ge, X. Li, H. Feng, C. Xu, Y. Lu, B. Chen, D. Li, C. Xu, Analysis of the pyrolysis process, kinetics and products of the base components of waste wind turbine blades (epoxy resin and carbon fiber), J. Anal. Appl. Pyrolysis 170 (2023) 105919, https://doi.org/10.1016/j.jaap.2023.105919.
[13] J. Eimontas, N. Striūgas, M. Praspaliauskas, M.A. Abdelnaby, Catalytic pyrolysis and kinetic study of glass fibre-reinforced epoxy resin over CNTs, graphene and carbon black particles/ZSM-5 zeolite hybrid catalysts, J. Therm. Anal. Calorim. 148 (3) (2022) 897–912, https://doi.org/10.1007/s10973-022-11776-9.
[14] I. Kiminaitė, J. Eimontas, N. Striūgas, M.A. Abdelnaby, Recovery of phenol and acetic acid from glass fibre reinforced thermoplastic resin using catalytic pyrolysis process on ZSM-5 zeolite catalyst and its kinetic behaviour, Thermochim. Acta 715 (2022) 179293, https://doi.org/10.1016/j.tca.2022.179293.
[15] L. Mishnaevsky, K. Branner, H.N. Petersen, J. Beauson, M. McGugan, B.F. Sørensen, Materials for wind turbine blades: an overview, Materials 10 (11) (2017) 1285, https://doi.org/10.3390/ma10111285.
[16] B. Wang, X. Wang, N. Xu, Y. Shen, F. Lu, Y. Liu, Y. Huang, Z. Hu, Recycling of carbon fibers from unsaturated polyester composites via a hydrolysis-oxidation synergistic catalytic strategy, Compos. Sci. Technol. 203 (2021) 108589, https://doi.org/10.1016/j.compscitech.2020.108589.
[17] T. Prabhuram, S. Singh, D.E. Raja, J.I. Durairaj, M.C. Das, P. Ravichandran, Development and mechanical characterization of jute fibre and multi-walled carbon nanotube-reinforced unsaturated polyester resin composite, Mater. Today: Proc. (2023), https://doi.org/10.1016/j.matpr.2023.08.302.
[18] J. Eimontas, N. Striūgas, M.A. Abdelnaby, Pyrolysis kinetic behaviour and thermodynamic analysis of waste wind turbine blades (carbon fibres/unsaturated polyester resin), Energy Sources Part A: Recovery Util. Environ. Eff. 45 (4) (2023) 10505–10522, https://doi.org/10.1080/15567036.2023.2246422.
[19] S. Yousef, J. Eimontas, N. Striūgas, et al., Recovery of styrene from waste wind turbine blades (fiberglass/polyester resin composites) using pyrolysis treatment and its kinetic behavior, J. Therm. Anal. Calor. 149 (2024) 521–538, https://doi.org/10.1007/s10973-023-12714-z.
[20] K. Zakarauskas, J. Eimontas, N. Striūgas, Recovery of styrene-rich oil and glass fibres from fibres-reinforced unsaturated polyester resin end-of-life wind turbine blades using pyrolysis technology, J. Anal. Appl. Pyrolysis 173 (2023) 106100, https://doi.org/10.1016/j.jaap.2023.106100.
[21] S. Yousef, J. Eimontas, I. Stasiulaitiene, K. Zakarauskas, N. Striūgas, Recovery of energy and carbon fibre from wind turbine blades waste (carbon fibre/unsaturated polyester resin) using pyrolysis process and its life-cycle assessment, Environ. Res. (New York, N.Y. Print) 245 (2024) 118016, https://doi.org/10.1016/j.envres.2023.118016.
[22] J. Huff, P.F. Infante, Styrene exposure and risk of cancer, Mutagenesis 26 (5) (2011) 583–584, https://doi.org/10.1093/mutage/ger033.
[23] N. Striūgas, J. Eimontas, M.A. Abdelnaby, Synthesis of value-added aromatic chemicals from catalytic pyrolysis of waste wind turbine blades and their kinetic analysis using artificial neural network, J. Anal. Appl. Pyrolysis 177 (2024) 106330, https://doi.org/10.1016/j.jaap.2023.106330.
[24] Y. Peng, Y. Wang, L. Ke, L. Dai, Q. Wu, K. Cobb, Y. Zeng, R. Zou, Y. Liu, R. Ruan, A review on catalytic pyrolysis of plastic wastes to high-value products, Energy Convers. Manag. 254 (2022) 115243, https://doi.org/10.1016/j.enconman.2022.115243.
[25] C.J. Wrasman, A.N. Wilson, O.D. Mante, K. Iisa, A. Dutta, M. Talmadge, D. C. Dayton, S. Uppili, M.J. Watson, X. Xu, M.B. Griffin, C. Mukarakate, J. A. Schaidle, M.R. Nimlos, Catalytic pyrolysis as a platform technology for supporting the circular carbon economy, Nat. Catal. 6 (7) (2023) 563–573, https://doi.org/10.1038/s41929-023-00985-6.
[26] I. Kiminaitė, J. Eimontas, N. Striūgas, M.A. Abdelnaby, Catalytic pyrolysis kinetic behaviour of glass fibre-reinforced epoxy resin composites over ZSM-5 zeolite catalyst, Fuel 315 (2022) 123235, https://doi.org/10.1016/j.fuel.2022.123235.
[27] K. Zakarauskas, J. Eimontas, N. Striūgas, A new sustainable strategy for oil, CH4 and aluminum recovery from metallised food packaging plastics waste using catalytic pyrolysis over ZSM-5 zeolite catalyst, Thermochim. Acta 713 (2022) 179223, https://doi.org/10.1016/j.tca.2022.179223.
[28] J. Hu, M. Danish, Z. Liu, P. Zhou, N. Zhu, H. Yuan, P. Qian, Effectiveness of wind turbine blades waste combined with the sewage sludge for enriched carbon preparation through the co-pyrolysis processes, J. Clean. Prod. 174 (2018) 780–787, https://doi.org/10.1016/j.jclepro.2017.10.166.
[29] C.C. Seah, C.H. Tan, N.A. Arifin, R. Hafriz, A. Salmiaton, S. Nomanbhay, A. H. Shamsuddin, Co-pyrolysis of biomass and plastic: circularity of wastes and comprehensive review of synergistic mechanism, Results Eng. 17 (2023) 100989, https://doi.org/10.1016/j.rineng.2023.100989.
[30] A. Saravanakumar, P. Vijayakumar, A.T. Hoang, E.E. Kwon, W. Chen, Thermochemical conversion of large-size woody biomass for carbon neutrality:

principles, applications, and issues, Bioresour. Technol. 370 (2023) 128562, https://doi.org/10.1016/j.biortech.2022.128562.
[31] S. Zhang, V.V. Badenko, I.K. Sosnovsky, V. Shamansky, A segmental analysis of pyrolysis of woody biomass, Thermochim. Acta 711 (2022) 179209, https://doi.org/10.1016/j.tca.2022.179209.
[32] X. Jin, J.H. Lee, J.W. Choi, Catalytic co-pyrolysis of woody biomass with waste plastics: Effects of HZSM-5 and pyrolysis temperature on producing high-value pyrolytic products and reducing wax formation, Energy 239 (2022) 121739, https://doi.org/10.1016/j.energy.2021.121739.
[33] G. Özsin, A.E. Pütün, Insights into pyrolysis and co-pyrolysis of biomass and polystyrene: thermochemical behaviors, kinetics and evolved gas analysis, Energy Convers. Manag. 149 (2017) 675–685, https://doi.org/10.1016/j.enconman.2017.07.059.
[34] A.C. Dyer, M.A. Nahil, P.T. Williams, Biomass:polystyrene co-pyrolysis coupled with metal-modified zeolite catalysis for liquid fuel and chemical production, J. Mater. Cycles Waste Manag. 24 (2) (2022) 477–490, https://doi.org/10.1007/s10163-021-01334-0.
[35] M. Wu, Z. Wang, X. Zeng, M. Zhang, T. Sun, Q. Wang, H. Zhu, S. Guo, Y. Chen, Y. Zhu, T. Lei, K.R.G. Burra, A.K. Gupta, Synergistic effects and products distribution during Co-pyrolysis of biomass and plastics, J. Energy Inst. 111 (2023) 101392, https://doi.org/10.1016/j.joei.2023.101392.
[36] K.R.G. Burra, A.K. Gupta, Kinetics of synergistic effects in co-pyrolysis of biomass with plastic wastes, Appl. Energy 220 (2018) 408–418, https://doi.org/10.1016/j.apenergy.2018.03.117.
[37] M. Alam, D. Rammohan, N.R. Peela, Catalytic co-pyrolysis of wet-torrefied bamboo sawdust and plastic over the zeolite H-ZSM-5: synergistic effects and kinetics, Renew. Energy 178 (2021) 608–619, https://doi.org/10.1016/j.renene.2021.06.109.
[38] H. Stančin, V. Strezov, H. Mikulčić, Life cycle assessment of alternative fuel production by co-pyrolysis of waste biomass and plastics, J. Clean. Prod. 414 (2023) 137676, https://doi.org/10.1016/j.jclepro.2023.137676.
[39] N. Striūgas, J. Eimontas, A. Mohamed, M.A. Abdelnaby, Pyrolysis kinetic behavior and thermodynamic analysis of PET nonwoven fabric, Materials 16 (18) (2023) 6079, https://doi.org/10.3390/ma16186079.
[40] S. Yousef, J. Eimontas, N. Striūgas, A. Mohamed, M. Praspaliauskas, M. A. Abdelnaby, Phenol and benzoic acid recovery from end-of-life of polysulfone ultrafiltration membranes and its thermochemical kinetic behaviour, Energy Sources Part A: Recovery Util. Environ. Eff. 45 (2) (2023) 6043–6061, https://doi.org/10.1080/15567036.2023.2213669.
[41] K. Slopiecka, P. Bartocci, F. Fantozzi, Thermogravimetric analysis and kinetic study of poplar wood pyrolysis, Appl. Energy 97 (2012) 491–497, https://doi.org/10.1016/j.apenergy.2011.12.056.
[42] Y.R. Wulandari, S.S. Chen, G.C. Hermosa, S.A. Hossain, Y. Yamauchi, T. Ahamad, S.M. Alshehri, K.C. Wu, H. Wu, Effect of N2 flow rate on kinetic investigation of lignin pyrolysis, Environ. Res. 190 (2020) 109976, https://doi.org/10.1016/j.envres.2020.109976.
[43] A. Aladin, B. Modding, T. Syarif, F. Dewi, Effect of nitrogen gas flowing continuously into the pyrolysis reactor for simultaneous production of charcoal and liquid smoke, J. Phys.: Conf. Ser. 1763 (1) (2021) 012020, https://doi.org/10.1088/1742-6596/1763/1/012020.
[44] K. Açıkalın, Determination of kinetic triplet, thermal degradation behaviour and thermodynamic properties for pyrolysis of a lignocellulosic biomass, Bioresour. Technol. (2021), https://doi.org/10.1016/j.biortech.2021.125438.
[45] R.K. Mishra, A.K. Sahoo, K. Mohanty, Pyrolysis kinetics and synergistic effect in co-pyrolysis of Samanea saman seeds and polyethylene terephthalate using thermogravimetric analyser, Bioresour. Technol. 289 (2019) 121608, https://doi.org/10.1016/j.biortech.2019.121608.
[46] S.P. Subadra, J. Eimontas, N. Striūgas, M.A. Abdelnaby, Thermal degradation and pyrolysis kinetic behaviour of glass fibre-reinforced thermoplastic resin by TG-FTIR, Py-GC/MS, linear and nonlinear isoconversional models, J. Mater. Res. Technol. 15 (2021) 5360–5374, https://doi.org/10.1016/j.jmrt.2021.11.011.
[47] M.A. Abdelnaby, J. Eimontas, N. Striūgas, Effect of aluminum leaching pretreatment on catalytic pyrolysis of metallised food packaging plastics and its linear and nonlinear kinetic behaviour, Sci. Total Environ. 844 (2022) 157150, https://doi.org/10.1016/j.scitotenv.2022.157150.
[48] I. Kiminaitė, J. Eimontas, N. Striūgas, M.A. Abdelnaby, Catalytic pyrolysis kinetic behaviour of glass fibre-reinforced epoxy resin composites over ZSM-5 zeolite catalyst, Fuel 315 (2022) 123235, https://doi.org/10.1016/j.fuel.2022.123235.
[49] J. Eimontas, N. Striūgas, M. Praspaliauskas, M.A. Abdelnaby, Pyrolysis kinetic behaviour, TG-FTIR, and GC/MS analysis of cigarette butts and their components, Biomass Convers. Bioref. (2022), https://doi.org/10.1007/s13399-022-02698-5.
[50] Eimontas Justas, Nerijus Striūgas, Mohammed Ali Abdelnaby, A new strategy for butanol extraction from COVID-19 mask using catalytic pyrolysis process over ZSM-5 zeolite catalyst and its kinetic behavior, Thermochim. Acta (2022), https://doi.org/10.1016/j.tca.2022.179198.
[51] M. Praspaliauskas, J. Striūgas, N. Zakarauskas, K, M.A. Abdelnaby, Pyrolysis kinetic behavior and TG-FTIR-GC–MS analysis of metallised food packaging plastics, Fuel 282 (2020) 118737, https://doi.org/10.1016/j.fuel.2020.118737.
[52] J. Eimontas, N. Striūgas, M.A. Abdelnaby, S. Yousef, Catalytic pyrolysis kinetic behavior and TG-FTIR-GC–MS analysis of metallized food packaging plastics with different concentrations of ZSM-5 zeolite catalyst, Polymers 13 (5) (2021) 702, https://doi.org/10.3390/polym13050702.
[53] A. Mohamed, J. Eimontas, N. Striūgas, M.A. Abdelnaby, Pyrolysis kinetic behavior and TG-FTIR-GC–MS analysis of end-life ultrafiltration polymer nanocomposite membranes, Chem. Eng. J. 428 (2022) 131181, https://doi.org/10.1016/j.cej.2021.131181.
[54] Z. Zhang, Y. Li, L. Luo, D. Yellezuome, M.M. Rahman, J. Zou, H. Hu, J. Cai, Insight into kinetic and thermodynamic analysis methods for lignocellulosic biomass pyrolysis, Renew. Energy 202 (2023) 154–171, https://doi.org/10.1016/j.renene.2022.11.072.
[55] J. Zhang, Y. Ding, W. Chen, C. Li, Y. Jiao, Pyrolysis kinetics, thermodynamics, and interaction analysis of co-pyrolysis of bituminous coal and electrolytic aluminum solid waste, Fuel 333 (2023) 126375, https://doi.org/10.1016/j.fuel.2022.126375.
[56] B. Gajera, U. Tyagi, A.K. Sarma, M.K. Jha, Pyrolysis of cattle manure: kinetics and thermodynamic analysis using TGA and artificial neural network, Biomass Convers. Bioref. (2023), https://doi.org/10.1007/s13399-023-04476-3.
[57] A. Nawaz, P. Kumar, Thermal degradation of hazardous 3-layered COVID-19 face mask through pyrolysis: kinetic, thermodynamic, prediction modelling using ANN and volatile product characterization, J. Taiwan Inst. Chem. Eng. 139 (2022) 104538, https://doi.org/10.1016/j.jtice.2022.104538.
[58] C. Ma, F. Zhang, J. Hu, H. Wang, S. Yang, H. Liu, Co-pyrolysis of sewage sludge and waste tobacco stem: gas products analysis, pyrolysis kinetics, artificial neural network modeling, and synergistic effects, Bioresour. Technol. 389 (2023) 129816, https://doi.org/10.1016/j.biortech.2023.129816.
[59] S. Verma, M. Kumar, R. Kaur, P. Kumar, M. Sillanpää, U.L. Štangar, Comprehensive study of the kinetics of combustion and pyrolysis of petrochemical sludge: experimentation and application of artificial neural network, J. Anal. Appl. Pyrolysis 174 (2023) 106140, https://doi.org/10.1016/j.jaap.2023.106140.
[60] M.M. Jaffar, M.A. Nahil, P.T. Williams, Pyrolysis-catalytic hydrogenation of cellulose-hemicellulose-lignin and biomass agricultural wastes for synthetic natural gas production, J. Anal. Appl. Pyrolysis 145 (2020) 104753, https://doi.org/10.1016/j.jaap.2019.104753.
[61] P. Bartocci, A. Anca-Couce, K. Slopiecka, S. Nefkens, N. Evic, S. Retschitzegger, M. Barbanera, C. Buratti, F. Cotana, G. Bidini, F. Fantozzi, Pyrolysis of pellets made with biomass and glycerol: kinetic analysis and evolved gas analysis, Biomass Bioenergy 97 (2017) 11–19, https://doi.org/10.1016/j.biombioe.2016.12.004.
[62] A.M. Saat, A.A. Malik, M.S. Kamil, M. Muslim, F.Z.B.Z. Azaim, A. Azmi, M.F. A. Latif, N.E.B. Ramlee, M.A. Ahmad, M.R. Johan, Thermal degradation of unsaturated polyester and composite fiberglass embedded with aluminium phosphate, Lect. Notes Mech. Eng. (2019) 117–124, https://doi.org/10.1007/978-981-15-0002-2_13.
[63] A.C. Dyer, M.A. Nahil, P.T. Williams, Biomass:polystyrene co-pyrolysis coupled with metal-modified zeolite catalysis for liquid fuel and chemical production, J. Mater. Cycles Waste Manag 24 (2022) 477–490, https://doi.org/10.1007/s10163-021-01334-0.
[64] S.P. Subadra, S. Tučkutė, A. Baltušnikas, I. Lukošiūtė, E.L. Arafa, A. Mohamed, Finite element analysis of fibreglass and carbon fabrics reinforced polyethersulfone membranes, Mater. Today Commun. 31 (2022) 103682, https://doi.org/10.1016/j.mtcomm.2022.103682.
[65] M. Praspaliauskas, J. Eimontas, N. Striūgas, M.A. Abdelnaby, Pyrolysis kinetic behaviour of glass fibre-reinforced epoxy resin composites using linear and nonlinear isoconversional methods, Polymers 13 (10) (2021) 1543, https://doi.org/10.3390/polym13101543.
[66] S. Singh, A. Tagade, A. Verma, A. Sharma, S.P. Tekade, A.N. Sawarkar, Insights into kinetic and thermodynamic analyses of co-pyrolysis of wheat straw and plastic waste via thermogravimetric analysis, Bioresour. Technol. 356 (2022) 127332, https://doi.org/10.1016/j.biortech.2022.127332.
[67] S. Yousef, J. Eimontas, N. Striūgas, M.A. Abdelnaby, Pyrolysis kinetic behaviour and TG-FTIR-GC–MS analysis of coronavirus face masks, J. Anal. Appl. Pyrolysis 156 (2021) 105118, https://doi.org/10.1016/j.jaap.2021.105118.
[68] L.B. Manfredi, E. Rodríguez, M. Władyka-Przybylak, A. Vázquez, Thermal degradation and fire resistance of unsaturated polyester, modified acrylic resins and their composites with natural fibres, Polym. Degrad. Stab. 91 (2) (2006) 255–261, https://doi.org/10.1016/j.polymdegradstab.2005.05.003.
[69] S. Yousef, J. Eimontas, N. Striūgas, M. Praspaliauskas, M.A. Abdelnaby, Pyrolysis kinetic behaviour of glass fibre-reinforced epoxy resin composites using linear and nonlinear isoconversional methods, Polymers 13 (10) (2021) 1543, https://doi.org/10.3390/polym13101543.
[70] A. Shajkumar, S.K. Samal, S. Mohanty, S.K. Nayak, The degradation and recycling of unsaturatedpolyester resin-based composites, in: Elsevier eBooks, 2019, pp. 599–610. ⟨https://doi.org/10.1016/b978-0-12-816129-6.00023-5⟩.
[71] K. Akubo, M.A. Nahil, P.T. Williams, Co-pyrolysis–catalytic steam reforming of cellulose/lignin with polyethylene/polystyrene for the production of hydrogen, Waste Dispos. Sustain. Energy 2 (3) (2020) 177–191, https://doi.org/10.1007/s42768-020-00047-8.
[72] K.P. Kumar, S. Srinivas, Catalytic co-pyrolysis of biomass and plastics (polypropylene and polystyrene) using Spent FCC catalyst, Energy Fuels 34 (1) (2019) 460–473, https://doi.org/10.1021/acs.energyfuels.9b03135.
[73] P.N.Y. Yek, Y.H. Chan, S.Y. Foong, W. a W. Mahari, X. Chen, R.K. Liew, N. Ling, Y. F. Tsang, C. Sonne, Y.W. Cheng, Y.H. Tan, S.S. Lam, Co-processing plastics waste and biomass by pyrolysis–gasification: a review, Environ. Chem. Lett. (2023), https://doi.org/10.1007/s10311-023-01654-7.
[74] Z. Wang, S. An, J. Zhao, P. Sun, H. Lyu, W. Kong, B. Shen, Plastic regulates its co-pyrolysis process with biomass: influencing factors, model calculations, and

mechanisms, Front. Ecol. Evol. 10 (2022), https://doi.org/10.3389/fevo.2022.964936.

[75] J. Eimontas, N. Striūgas, M.A. Abdelnaby, Influence of carbon black filler on pyrolysis kinetic behaviour and TG-FTIR-GC–MS analysis of glass fibre reinforced polymer composites, Energy 233 (2021) 121167, https://doi.org/10.1016/j.energy.2021.121167.

[76] G. Özsin, A.E. Pütün, Co-pyrolytic behaviors of biomass and polystyrene: kinetics, thermodynamics and evolved gas analysis, Korean J. Chem. Eng. 35 (2) (2017) 428–437, https://doi.org/10.1007/s11814-017-0308-6.